Dynamic Motion Analysis of Aorta

: Image Processing Methods for MDCT and Cine-MR Image

Hun Shim

The Graduate School

Yonsei University

Department of Biomedical Engineering

Dynamic Motion Analysis of Aorta

: Image Processing Methods for MDCT and Cine-MR Image

A Dissertation
Submitted to the Department of Biomedical Engineering
and the Graduate School of Yonsei University
in partial fulfillment of the
requirements for the degree of
Doctor of Philosophy

Hun Shim

December 2011

This certifies that the dissertation of Hun Shim is approved.

Young Ro Yoon: Thesis Supervisor

Taemin Shin: Thesis Committee Member #1

Dae Sung Yoon: Thesis Committee Member #2

Jong-Won Ha: Thesis Committee Member #3

Young Jin Kim: Thesis Committee Member #4

The Graduate School

Yonsei University

December 2011

Acknowledgements

First and foremost, I would like to thank my parents for always believing in me and providing me with love and encouragement. I also thank my brother Hyun Shim for his support.

I would like to thank my advisor, Dr. Young Ro Yoon, for giving me the opportunity to fulfill my goal and providing me with the guidance to successfully finish my dissertation. I thank all members of my dissertation committee, Dr. Taemin Shin, Dr. Dae Sung Yoon, Dr. Jong-Won Ha, and Dr. Young Jin Kim for their critique and advice.

I would like to thank all past and present members of the Biomedical Signal Processing Laboratory, Dr. Hong Mo Seong, Dr. Jae Woo Shin, Dr. Seung Jin Jang, Kyu-Seog Hong, Yong Gu Jang, Jeong Hoon Yi, Seung Hwan Lee, Hyun Chul Ko, Chun Hee Hong, Jong Hyuk Kim and Jung Hyun Heo for their help with the projects as well as their friendship.

I would like to thank Dr. Chungkeun Lee for his tremendous support as a research partner.

I heartily thank my wonderful colleagues in Yonsei University; Dr. Incheol Jung, Dr. Sung Pil Cho, Dr. Youngwoo Bae, Hyoki Lee, Chang Min Yeo, and Yunjin Bae.

I would like to thank my friends, Jin Heo, Kyungwan Kay Ro, Shin Young Lee, Duck Yong Kim, Min Sang Park and Sung Man Heo.

I would like to thank Kyung Ok Lim. I could not have accomplished this without her love and support.

Finally, I would like to thank my aunt and uncle – Dr. Jang Yeon Kwon, Dr. Young Uh - for their endless love and support.

Table of Contents

List of Figures

List of Tables

Abstract

Dynamic Motion Analysis of Aorta

: Image Processing Methods for MDCT and Cine-MR Image

Hun Shim
Department of Biomedical Engineering
The Graduate School
Yonsei University

This dissertation was to study on image processing method for dynamic motion analysis of aorta using sequential images. The visualization of blood vessel motion and imaging protocols for cross-sectional aorta images are proposed.

To accomplish assess the aorta motion, muti-steps image processing strategy was applied. First, the image pre-processing was applied to image enlargement and segmentation of aorta. Second, the intensity profile of aorta was used for wall boundary extraction. Third, semi-automatic extraction of target aorta boundary tracing over first frame is then automatically tracked throughout the image frames. The visualization of aorta motion in the sequential images provides a quantitative source of

their motion in space. In order to visualize the blood vessel wall motion, velocity vector mapping was applied to the sequential images. It provided the information of aorta wall movement velocity and aortic displacement.

To evaluate the proposed methods, clinical validation have been designed using MDCT and Cine-MR images.

The aortic wall movement property, the movement profiles on aorta calcification, aortic displacement, and relations between wall movement and age were assessed using MDCT images. The number of subjects (14 men, 16 women; mean age, 55.9 ± 14.99 years; range, 31-80 years) were 30 and have valvular heart disease. The correlation between wall movement at three different position of thoracic aorta and entire study population group was -0.63 ($p < 0.001$), -0.51 ($p < 0.05$) and -0.45 ($p < 0.05$) respectively. The profiles of wall variation in aorta calcification indicate dyssynchoronous aorta expansion. The clusters which are include the calcification point showed low variation throughout the image samples.

The aortic wall movement of Turner syndrome group were also assessed using Cine-MR images. The number of subjects (17 women; mean age, 21.6 ± 6.6 years; range, 11-38 years) were 17. The wall movement data of total subjects were presented as mean ± standard deviation. The movement of descending aorta at three different position were 0.79 ± 0.25, 0.59 ± 0.15 and 0.53 ± 0.15 respectively.

There was a significant decrease of the aortic wall motion at all thoracic levels throughout the ages. Although specific assessment of vascular aging

was not available for the diseased subjects, a potential distinction on the aorta aging at the different ages was possible.

In contrast to the ascending aorta, the descending segments presented a significantly lesser magnitude of displacement and appear rather fixed at their thoracic position.

The results of this dissertation provide the fundamental characteristics of blood vessel motion and could be used not only clinical researches also clinical applications, such as vascular aging, assessment of vascular disease, and early detection of vascular abnormality.

Key Words : blood vessel assessment, aorta motion, multidetector computed tomography, magnetic resonance imaging, vector velocity

Chapter 1

1. Introduction

This chapter presents the motivation for this dissertation, an overview of the structure of the study and its main contributions.

This dissertation presents setting up the evaluation method of aorta obtained by MDCT and MR images. The method includes aorta segmentation, measurement of wall movement and displacement of aorta.

Automated techniques for the segmentation of aorta not only provide better visualizations but also enable mechanical properties.

1.1. Motivation

1.1.1. Non-invasive Vascular Imaging in Diagnosis

Vascular imaging is a medical imaging technique used to visualize the inside with particular interest in blood vessels [1-3].

The technique to image has changed from conventional invasive vascular imaging by means of catheters to non-invasive vascular imaging [4]. The

development of cross-sectional imaging modalities such as ultrasound imaging (US) [5-6], computed tomography (CT) [7-8], and magnetic resonance (MR) imaging [9-10] has provided the medical community for non-invasive blood vessels imaging environments. The cross-sectional imaging of vascular gives additional information about the vessel wall and the surrounding tissue [11]. It has significantly decreased the risk of vessel trauma and procedural time [12].

The vascular imaging has also come to play a major role in the disease diagnosis. Vascular such as carotid artery and aorta diseases are one of the leading causes of death worldwide. That field has progressed rapidly over the last one century. Those improvements have contributed to advancements diagnosis and treatment as well as to a better understanding of vascular diseases. Non-invasive blood vessel imaging is used for the diagnosis of cardiovascular, cerebrovascular, and peripheral vascular disease [13-15].

1.1.2. Necessity of Vascular Assessment

Prompt and accurate diagnosis has been shown to greatly influence treatment planning of vascular diseases. The advances in different imaging modalities as well as contrast media, for example, vascular ultrasound, multi-detector computed tomographic angiography (MDCTA) [16] and magnetic resonance angiography (MRA) [17-18] potentially enable the non-invasive, effective, and accurate diagnosis of most vascular related diseases. Consequently, the interpretation of images from various vascular

imaging modalities is a demanding task. Recently, there has been tremendous interest in the field of the development of advanced image analysis methods for the enhancement, segmentation, and visualization of the vasculature as well as the quantitative risk assessment/prediction and treatment planning of vascular diseases. The integration of post-processing techniques with the various imaging modalities can be useful to increase the efficacy and accuracy for vascular disease assessment, thus potentially reducing the mortality rate.

1.2. Objectives

The objectives of this dissertation are to investigate the feasibility and limitation of the wall motion tracking for cross-sectional vascular imaging in MDCT and MR. To accomplish this, image acquisition protocols and wall motion tracking methods were proposed.

Therefore, the focus could be on the area of vascular imaging and image processing techniques, as well as the fusion of multi-modality

The objectives of this dissertation are following

- To propose semi-automatic image processing method in order to extract the vascular boundary and wall motion information of blood vessel images from MDCT and MR images
- To establish imaging protocols that can assess wall motion of aorta

- To evaluate the performance of proposed method with clinical image data

1.3. Outline of Dissertation

The development of evaluation method and obtain reference data for aorta wall movement is the goal of this dissertation. This dissertation consists of seven chapters.

Chapter 2 introduces the anatomy of aorta. The aortic diseases are also discussed.

Chapter 3 presents the non-invasive vascular imaging background for this dissertation. It presents a brief overview of the MDCT and MR angiography related to the dissertation.

Chapter 4 introduces the experimental setup to assess the aorta in MDCT and MR. It discusses also image acquisition protocol in each modality.

Chapter 5 describes the evaluation method aorta wall movement. Detailed descriptions of the necessary pre-processing steps, aorta segmentation method, aorta wall selection and velocity vector mapping for aorta movement analysis are provided. The parameters for measuring aorta characteristic are also presented.

Chapter 6 describes the clinical data validation to assess the aorta motion using MDCT and MR images.

Chapter 7 presents conclusions and future work briefly.

Chapter 2

2. Aorta Anatomy and Disease

This chapter is consists of two sections. This chapter describes anatomical information of aorta and vascular related disease to understand this dissertation. Section 2.1 ‘Anatomy of Aorta’, introduces the anatomy of aorta. Section 2.2 ‘Aortic Disease’, explains the cause of aorta disease and symptoms.

2.1. Anatomy of Aorta

The aorta is the largest artery in the body. The vessel is originating from the left ventricle of the heart and extending down to the abdomen, where it branches off into two smaller arteries. The aorta delivers oxygenated blood to all tissues of the body through the systemic circulation. The size and the shape of aorta differ significantly among individuals and even within the same individual at different age.

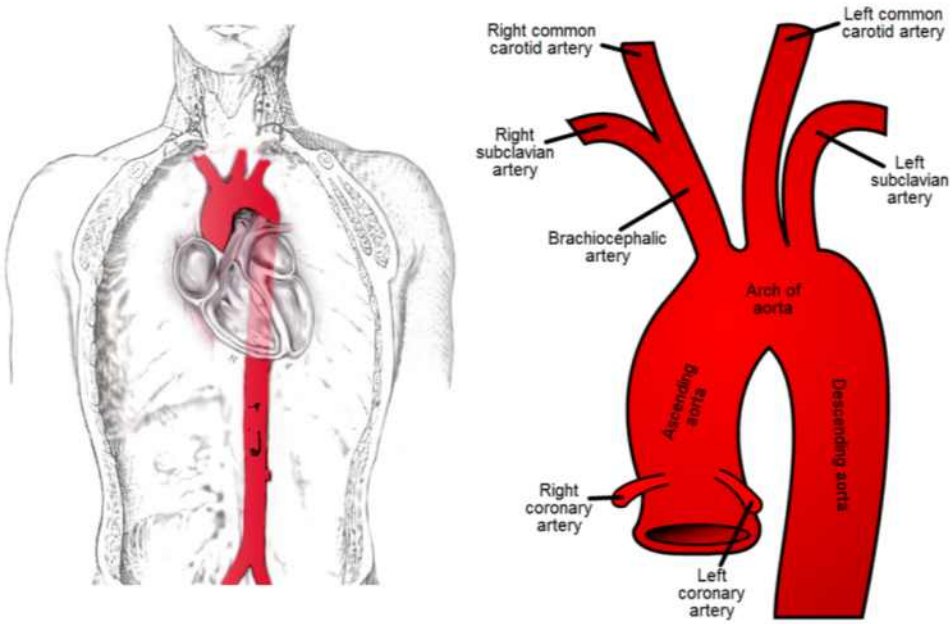

Figure 2.1 Anatomy of human aorta (image from Stedman's Medical Dictionaries)

The aorta is an elastic artery, and as such is quite distensible [19-20]. The blood pressure is highest (normal blood pressure is a reflection of aortic blood pressure) and most pulsatile in the aorta, as blood pressure decreases and becomes more smooth (and less pulsatile) as the blood travels from aorta to arteries to arterioles to capillaries, where metabolic exchange occurs. The aorta consists of a heterogeneous mixture of smooth muscle, nerves, intimal cells, endothelial cells, fibroblast-like cells, and a complex extracellular matrix. The vascular wall consists of several layers known as the tunica adventitia, tunica media, and tunica intima. The thickness of the aorta encourages an extensive network of tiny blood vessels called vaso vasorum, which feed the layers of the aorta.

The aorta is usually divided into five segments as follows:

· Ascending aorta: the section between the heart and the arch of aorta

· Arch of aorta: the peak part that looks somewhat like an inverted "U"

· Descending aorta: the section from the arch of aorta to the point where it divides into the common iliac arteries

· Thoracic aorta: the half of the descending aorta above the diaphragm

· Abdominal aorta: the half of the descending aorta below the diaphragm

2.2. Aortic Disease

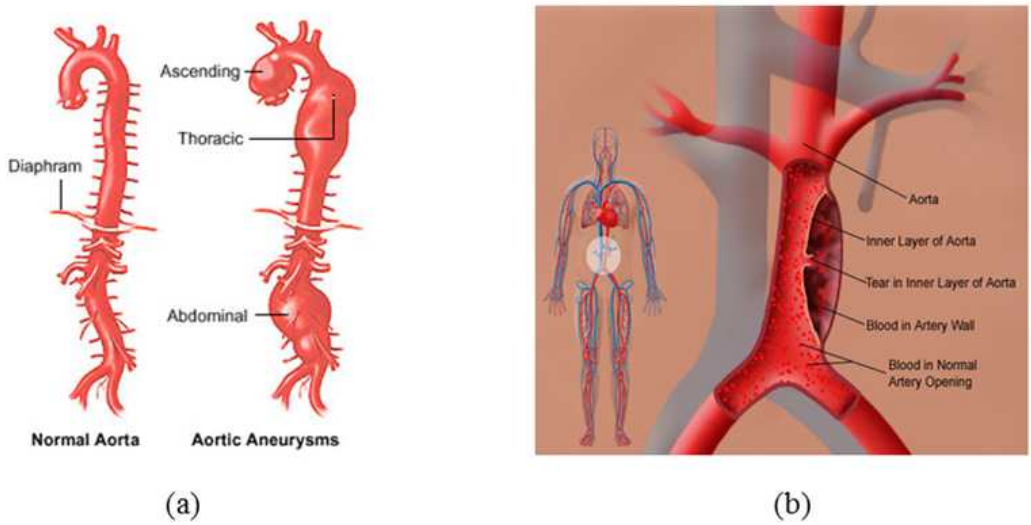

Figure 2.2 Aortic disease (a) aortic aneurysm (b) aortic dissection (image from Yale Medical Group)

The aorta is the largest artery that carries blood and nutrients from the heart to the rest of the body. Like the other most arteries, the aorta is elastic, which allows it to be filled with blood under high pressure.

Aortic disease is a form of peripheral artery disease that affects the aorta, the main blood vessel in the body. The most common problem is an aortic aneurysm. It is an enlargement of the lower part of the aorta that extends through the abdominal area. When it reaches a certain size this enlarged area is referred to as an aneurysm. Traditionally for the aorta, any permanently dilated section measuring 4.0 cm or greater in diameter has

been regarded as aneurysm. This area tissue is formed by degeneration of the cells composing the aortic wall. This damaged tissue is weak, lacking sufficient elastic components to stretch and contract well. Aortic Aneurysms usually are discovered before they produce symptoms, such as back pain, but like the weakened hose, they may rupture if they become too large.

Aortic tissue may also tear. Tearing of the inner layer of the vessel wall allows blood to leak into the middle layer of the aorta, separating the inner and outer layers. This is called dissection [21].

Thoracic aortic dissection can be generated by risk factors such as bicuspid aortic disease, Marfan syndrome and Ehlers-Danlos syndrome, other connective tissue disorders (Marfanoid), atherosclerosis, miscellaneous infectious and inflammatory conditions, hypertension, smoking, trauma [22-23]. Since a ruptured aneurysm is extremely dangerous and can cause life-threatening bleeding, aneurysms are best corrected by an operation before this happens.

Chapter 3

3. Non-invasive Vascular Imaging

This chapter describes basic background information to understand imaging modality. It consists of three sections. Section 3.1, 'Imaging Modality', present brief conventional and current MDCT and MR in medical fields. Section 3.2, 'Vascular Imaging', explains the major role in MDCT and MR angiography field. Finally, section 3.3, 'Vascular Validation Method' presents the current study of blood vessel evaluation briefly.

3.1. Imaging Modality

3.1.1. Basic Principles of MDCT Imaging

This section reviews fundamentals of MDCT detectors, single and dual source configurations, spatial and temporal resolution and image noise briefly.

Computed tomographic angiography (CTA) is a test that combines the

technique of a conventional computed tomography (CT) scan with the method of traditional angiography to detailed images of the blood vessels in the body. CTA is an important imaging modality in the evaluation of the vascular system throughout the body. With the advent of multi-detector computed tomography (MDCT), CTA seems to be superior even to conventional angiography in certain vascular studies [24-26]. The MDCT compared with conventional CT has several advantages in technical aspects. It is providing greater anatomical coverage than was previously available, reduced image acquisition time, isotropic voxel acquisition, and rapid target acquisition in one shot [27-28]. It also provides consuming fewer resources, and being more cost-efficient. With the recent introduction of 128-MDCT in cardiac imaging, the temporal and spatial resolution of CT angiography has improved [29-31].

Despite striking advances, MDCT has limitations. One of the major challenges of MDCT is dealing with the blizzard of data, which is mostly related to the increased number of examinations and the ever greater amount of information generated per examination [32-33]. Consequentially, semi-automatic and automatic functionalities for doctors should be present, such as heart, vessels extraction and tissue removal for cardiac studies.

After the introduction of CT in the late 1980s, imaging of the aorta soon became a routine procedure for evaluation of the aorta in patients with aortic relevant disease such as aortic dissection, stenosis or aneurysm formation [34-36].

According to the recent studies, understanding pathologic changes in aorta is essential. Calcified aorta is a risk factor for cardiovascular disease (CVD), as it has been associated with coronary artery disease, carotid artery disease and stroke in the general population [37]. It has also been associated with heart failure [38-39]. Increased aortic stiffness is related to aortic calcification. It leads to left ventricular hypertrophy, left ventricular diastolic dysfunction, myocardial fibrosis and subsequent congestive heart failure and sudden death. Aortic calcification has relevance to age, hypertension and history of cardiovascular disease [40-42].

Pathologic changes in aorta have been associated with various CVD. Knowing basic normal parameters such as diameter, area and shape is important to detect abnormality. The recent MDCT provides excellent accuracy and reproducibility.

Over the last decade, CT technology has developed rapidly with the introduction of MDCT to the clinical practice. Demand for better technology continues to drive vendors to develop further innovations in very short time periods. As a result, it has become difficult for many radiologist, physicians and technologists to keep up with speed of development. The advances in MDCT scanning have resulted in numerous variations of 4-320 channel MDCT modalities being available on the market and in use all over the world. In order to achieve your imaging purposes, interpreting physicians must thoroughly understand the attributes and capabilities of the type of modalities in their hospitals.

Single detector CT was first utilized in the early 1970's. In the 1980s four channel MDCT was introduced in practical use. Since that generation, the addition of more imaging channels, detectors has increased exponentially. Multiple detector rows permit high-resolution with short overall data acquisition time. Currently, 128-MDCT is considered state-of-the-art for cardiac imaging, whereas 256 and 320-MDCT systems are being developed.

When imaging an object with MDCT scanners, temporal and spatial resolution are important. Firstly, temporal resolution is defined as the length of time required to image a structure. In order to image a moving object with a high degree of temporal resolution, without little motion artifacts, one must acquire the image faster than that object is moving. It is important when imaging anatomy that moves, such as the heart and coronary arteries. The increased gantry rotation speed, together with dedicated ECG-gated image reconstruction algorithms, provides for high temporal resolution. Consequently, it is possible to obtain phase-correlated image data sets. The ECG-gated 4-MDCT is introduced around the year 2000 [43-44]. The modality was providing the scanning ability for mechanical evidence of the heart and coronary arteries. However, it has a limitation due to insufficient temporal resolution. The major manufacturer currently offers a 64 channel MDCT scanner with ECG-gating software for cardiac imaging. Secondly, spatial resolution is defined as the ability to distinguish two objects as separate from one another. It has relevance to

speed of tube rotation, focal spot size, detector size and the distance between the focal spot and the detector ring [45].

The most powerful advantage of MDCT is the acquisition of multiple thin slices in the exploration of large volumes. The slices are acquired in a very short time and have a high longitudinal spatial resolution. Reduced scan duration improves image quality and removes motion artifacts in patients. Figure 3.1 shows the example of MDCT scanners.

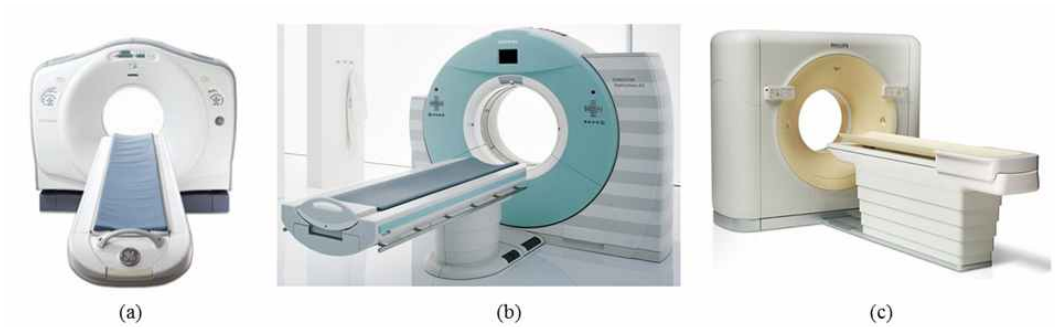

Figure 3.1 MDCT scanners (a) GE Healthcare, LightSpeed CT750 HD (b) SIEMENS, Somatom Definition AS (c) Philips, Brilliance CT 16 Slice

3.1.2. Basic Principles of MR Imaging

MRI uses the magnetic properties of hydrogen and its interaction with both a large external magnetic field and radio waves to produce highly detailed images of the body. Figure 3.2 shows the MRI scanners and principles.

The field strength of the magnets used for MR is measured in units of Tesla (T). One Tesla is equal to 10,000 Gauss. The magnetic field of the earth is approximately 0.5 Gauss. Given that relationship, a 1.0 T magnet has a magnetic field approximately 20,000 times stronger than that of the earth.

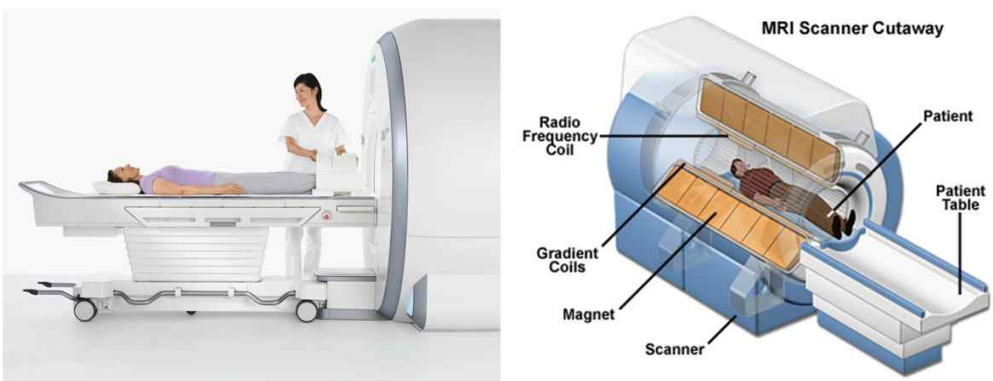

Figure 3.2 MRI Scanner and principles (image from PANOPTES)

MR images can be enhanced by the use of contrast agents. The contrast agents for MRI have paramagnetic properties, such as gadolinium and manganese, used to alter tissue relaxation times. MRI is the best suited for cases when a patient is to undergo the exam many times successively in

the short term. MRI can generate cross-sectional images in any plane including oblique planes [46-48].

In medical practice, MRI is used to distinguish pathologic tissue such as tumor, cancer from normal tissue. One advantage of an MRI scan is that it is harmless to the subjects. It uses strong magnetic fields and non-ionizing radiation in the radio frequency range. Compare this to traditional X-rays which involve doses of ionizing radiation and may increase the risk of malignancy [49-51].

3.2. Vascular Imaging

3.2.1. Vascular Imaging with MDCT

CTA is a computed tomography technique used to visualize arterial and venous vessels throughout the body. This method displays the anatomical detail of blood vessels more precisely. The rapid technique growth in cardiac MDCT is result of exploring further advanced imaging concept. Present and potential future options in cardiac MDCT are discussed briefly in this section.

MDCT angiography (MDCTA) has many benefits as a noninvasive diagnostic modality. Measurement of a cross-sectional area of vessels will improve diagnostic accuracy. Figure 3.3 shows the CTA of the chest.

Cardiac angiography by MDCT includes detection of calcium scoring in coronary artery, anomalous coronary artery origins, and identification of myocardial bridging. Vascular injury such as aneurysm and dissection in aorta can be detected with MDCTA.

High spatial resolution and low image noise achievable with MDCT makes this system perfect for depicting normal and abnormal morphology of heart. The structure of heart, its chambers, arterial and venous connections, valves and the myocardium are clearly displayed.

Figure 3.3 Courtesy of Siemens SOMATOM Sensation, CT Angiography of the Chest (a) Normal origin and course of right coronary artery seen (b) Diffuse plaque noted in the left coronary artery

Wall motion can be detected when the heart has been scanned using retrospective ECG-gating because the entire cardiac cycle will have been depicted. When viewed in standard cardiac imaging planes, physician can evaluate the myocardial wall motion just as is done with echocardiography and MRI. Functional assessment of wall motion abnormalities may contribute to diagnosis of disease.

MDCT cardiac imaging is providing precise anatomic knowledge of the widely variant anatomy of the venous ostium, branching pattern and the shape. The accurate anatomic information can be integrated with angiographic image data. In the case of aneurysm and dissection, the

imaging of thoracic aorta may need to be investigated.

The improved MDCT performance leads to development of image reconstruction such as maximum intensity projections (MIPs), multi-projection volume reformation (MPVRs), minimum intensity projections (miniIPs) and volume rendering techniques (VRTs). Although, all these tools are listed by all vendors, their actual performances differ significantly.

3.2.2. Vascular Imaging with MR

Many of Cardiac MRI applications are commonly employed in clinical practice for example, in the evaluation of congenital heart disease, cardiac masses, the pericardium, right ventricular dysplasia, and hibernating myocardium [52-55]. In addition, other applications such as evaluation of myocardial perfusion and of valvular and ventricular function are very accurately evaluated with MRI [56].

MRA is a bundle of techniques based on MRI to image blood vessels. MRA is often used to evaluate the arteries of the neck and brain, the thoracic and abdominal aorta, the renal arteries. It generates pictures of the arteries to evaluate them for stenosis and aneurysms. Techniques like phase contrast angiography can also be used to generate flow velocity maps easily and accurately [57-58].

Contrast enhanced MRA (CE-MRA), Phase-contrast MRA (PC-MRA) and Time of Flight (TOF) MRA will briefly introduces below.

CE-MRA is currently the most common method of acquiring MRA. The contrast agent is injected into a vein, and images are acquired during the first pass of the medium through the arteries. This method provides the correct timing this may result in images of very high quality. Since longer time is available for image acquisition process, higher resolution imaging is possible. However, problem is the fact that both arteries and veins are enhanced at the same time if higher resolution images are required.

PC-MRA is manipulated by special varying magnetic fields that are preset to a maximum expected flow velocity. An image acquisition that is reverse of the bipolar gradient is then acquired and the difference of the two images is calculated. Static tissues such as muscle or bone will subtract out, however moving subject such as blood will acquire a different phase since it moves continuously through the gradient. The strength of the technique is that in addition to imaging the flowing blood, quantitative measurements of blood flow occur at the same time.

TOF MRA is the flow compensated gradient-echo sequences will be optimized to favor the vascular signal over that of the surrounding tissues by favoring the inflow effect. Because of the blood flowing into the explored zone has not been saturated, its longitudinal magnetization is maximal. The signal from the blood flow is thus stronger than that of the saturated tissues.

Figure 3.4 and 3.5 introduces the examples of MRA.

Figure 3.4 Contrast enhanced MRA of the renal arteries to evaluate for renal Artery stenosis (image from article: MR Imaging of aortic and peripheral vascular disease)

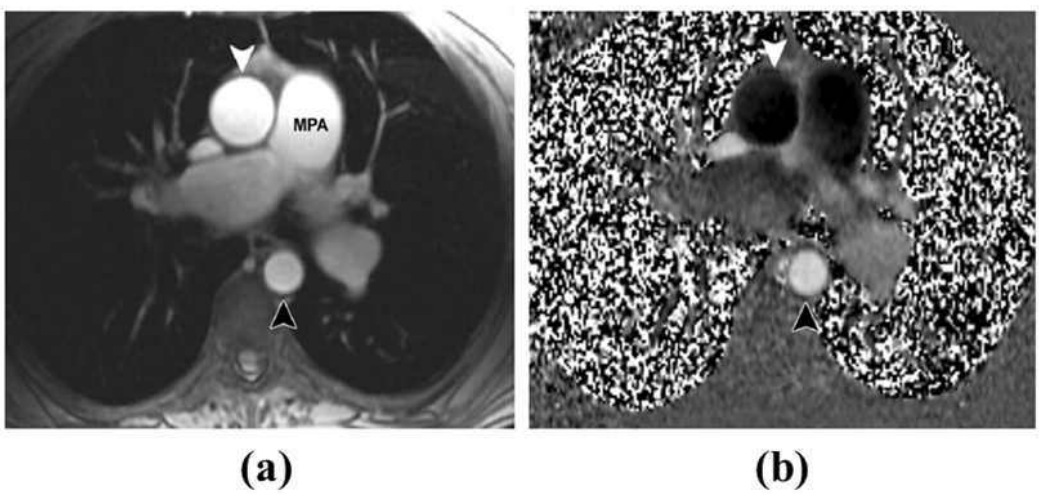

Figure 3.5 Phase-contrast imaging of the aorta. Magnitude (a) and phase (b) axial images show the ascending (image from article: MR Imaging of aortic and peripheral vascular disease, RadioGraphics, S. Tatli et al.)

3.3. Vascular Validation Method

The blood vessel wall motion velocity is derived as the ratio between frame-to-frame displacements and the time interval [59-61]. The velocity vectors in the 2-D plane are displayed throughout the cardiac cycle, representing both the magnitude of the velocity and the direction of the motion. Strain and strain rate (SR) [62-63] are obtained by comparing displacement of the speckles in relation to each other along the blood vessel contour throughout the cardiac cycle.

A number of features have been developed to characterize cardiac motion in order to detect cardiac wall motion abnormalities, among them: velocity, radial and circumferential strain, local and global Simpson volume. The following is a basic description of some of the features [64-66].

Velocity features: determines how fast any pair of control points change in the x and y coordinate system per frame.

Circumferential strain features: also called Fractional shortening, measures how much the contour between any two control points shrinks in the systolic phase. This is measured along the parameter of the contour.

Radial strain features: also called Thickening, measures how much the contour shrinks for each control point between any two time frames. This is measured along the radius from a calculated “center” of the left ventricle.

Chapter 4

4. Aorta Images Acquisition

This chapter is consists of two sections. Section 4.1 ‘MDCT Imaging Protocol’, introduces the experimental environment such as modality specifications, subjects and results of image acquisition. Section 4.2 ‘MR Imaging Protocol’, also describes the experimental environment to assess the aorta. The aim of this chapter is to investigate the differences when image produce using different image modalities.

4.1. MDCT Imaging Protocol

All experiments were performed using MDCT scanner. Most subjects were examined using SOMATOM Definition flash (Siemens, Germany) and remaining subjects were examined using Sensation 64 (Siemens, Germany).

Sensation 64 has increased rotation rate and acquiring 64 slices per gantry rotation. In addition, z-axis resolution was increased by a new z-flying focal spot technology. Further acquisition parameters were as

follows: detector collimation, 32x0.6 mm; gantry rotation, 285; temporal resolution, 75 ms; pitch 0.2 mm per gantry rotation; tube voltage, 120 kV; tube current, 1156 mAs. Temporal resolution depends on the number of rotation used for interpolation, heart rate, and scanner rotation time. Spatial resolution depends on the subjects examinations [67].

All images were reconstructed by an experienced observer. Successful post processing of angiographic data necessitates image acquisition of adequate quality. Image size was 512 by 512. The image frame was most twenty.

The images are obtained from three different positions for aorta evaluation: upper, middle, low at level of thoracic aorta. The positions and the images are shown in figure 4.1. The solid white rectangle in figure 4.1 is the ascending aorta, and the dashed red rectangle is the descending aorta. The ECG-gated MDCT images showed a high contrast between the contrast medium the aorta and the surrounding fatty tissue [68-69].

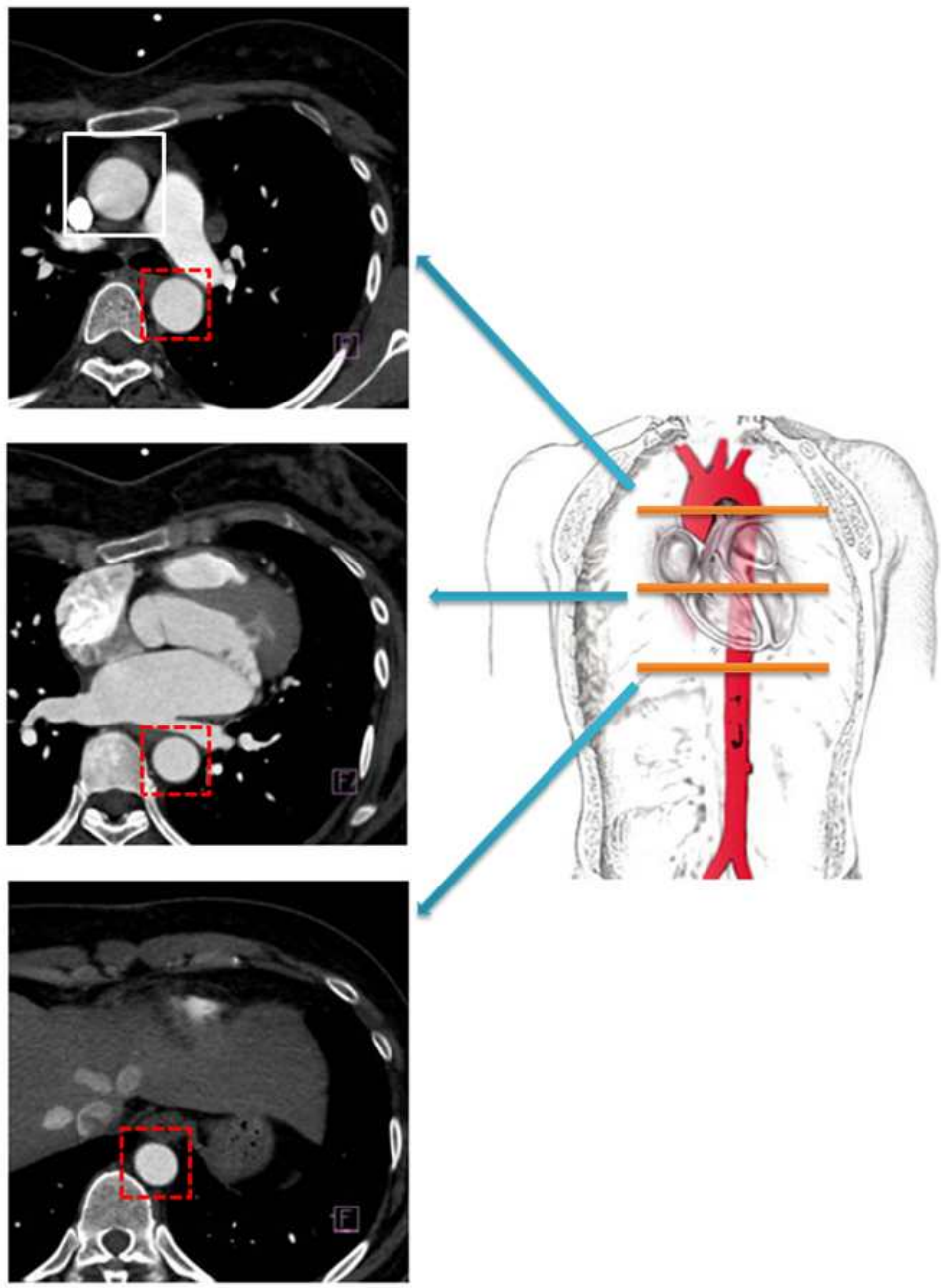

Figure 4.1 MDCT image samples and the three different positions of aorta

4.2. Cine-MR Imaging Protocol

Most patients were examined using a 1.5 T MRI system (Intera Achieva, Philips Medical Systems and Netherland). Spatial resolution: around 1.5 mm according to the subject examination. The image frame was most sixty.

The MR images of descending aorta were obtained in the axial planes. The image size is 256 by 256. The images are obtained from three different positions for aorta evaluation: upper, middle, low at level of thoracic aorta. Figure 4.2 shows the MR image samples and the three different positions of aorta. The solid white rectangle in figure 4.2 is the ascending aorta, and the dashed red rectangle is the descending aorta.

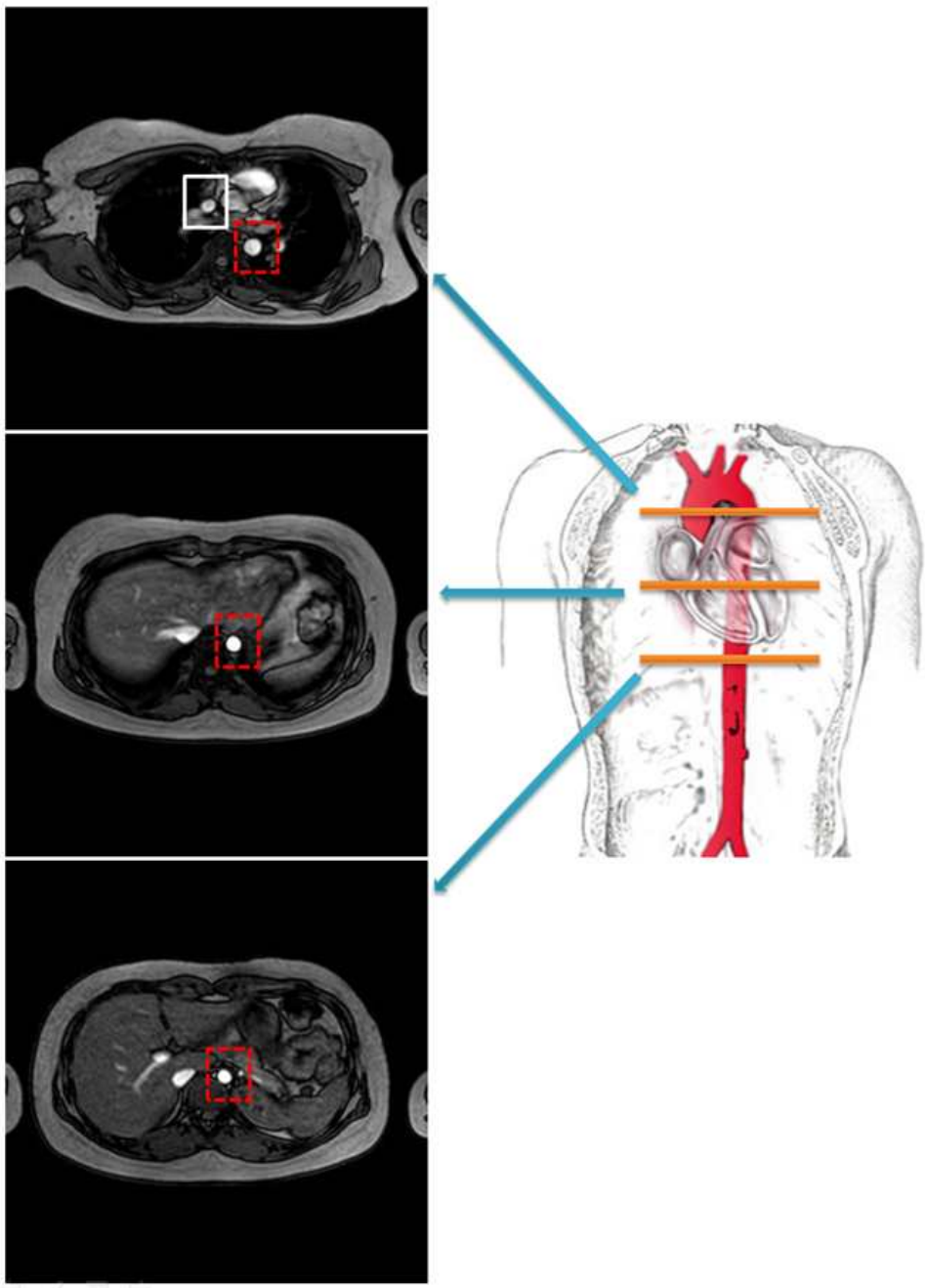

Figure 4.2 MR image samples and the three different positions of aorta

Chapter 5

5. Visualization of for Aorta Motion

This chapter is consists of four sections. Section 5.1 ‘Aorta Segmentation’, describes the work toward an automatic approach to identify the region of aorta in image dataset. Section 5.2 ‘Estimation of Aortic Wall’, introduces the lumen boundary extraction algorithm and results. Section 5.3 ‘Visualization of Aorta Motion’ explains the process of mapping the wall motion with image slices. It presents the procedures and the processing algorithms to track the vascular wall motion data from the sequential images. In addition, a detailed explanation about the evaluation method of target vascular will be given.

An MDCT scanner acquires one image at a time [70]. For each slice, multiple images (typically, 10 to 20) are acquired while the subjects hold their breath. Since the system is connected to an electrocardiogram, it knows exactly how the heart beats, so it can combine all the images for one slice to reconstruct the equivalent of one heart cycle.

The challenges in segmentation cardiac MR or CT images are multiple. We have developed various strategies to perform this task automatically

depending on the segmentation situation [71-73].

Figure 5.1 shows the overall procedure of proposed image process for wall motion tracking in this study.

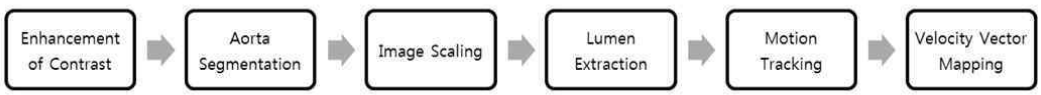

Figure 5.1 Image processing method for wall motion tracking

5.1. Aorta Segmentation

Since the aorta exists for different frames, repetitive structure elimination operations are required except aorta to compose vector velocity imaging of aorta wall motion. In this process, the aorta assumed circle.

Aorta detection uses Hough transform (HT). The HT is a standard method for shape recognition in image processing. It was first applied to detection of straight lines [74] and later extended to circles [75], ellipses [76], and arbitrarily shape objects [77]. Figure 5.2 show the basic principles of circular Hough transform.

The circular HT was introduced for detecting circles and circular arcs in digital images especially.

The basic principle of the CHT form is to fit circle to a portion of a curve, where x, y are image space, a, b the Hough space of the center of the circle, and r is its radius.

The following are the steps for aorta detection

1) Load image

2) Edge detection

3) For each edge point

3.1) For each value of r

3.1.1) Draw a circle with center in the edge point and radius r

3.1.2) Increment all points that the circle passes through

4) Find one or maxima in the images

Figure 5.3 shows the process aorta extraction using Circular Hough transforms and figure 5.4 shows the extracted sample aorta images from MDCT.

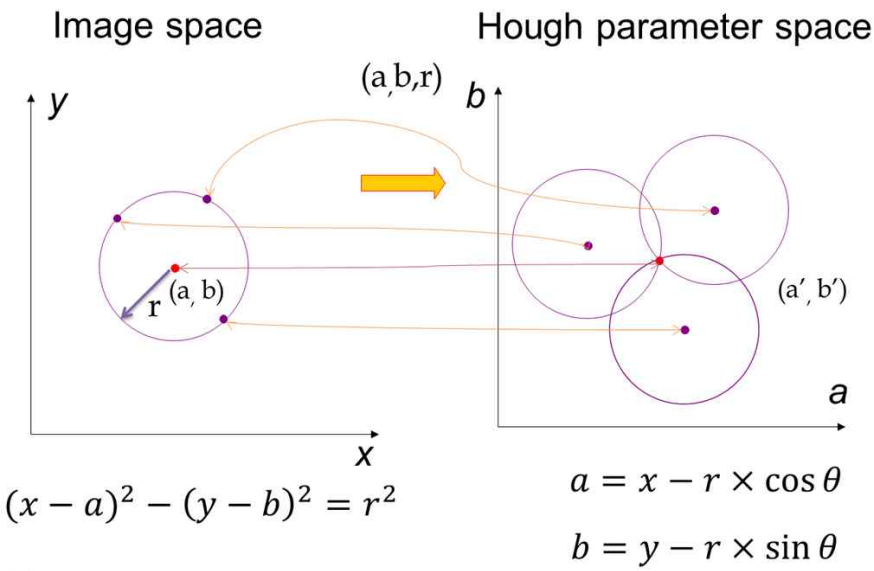

Figure 5.2 The basic principle of circular Hough transforms

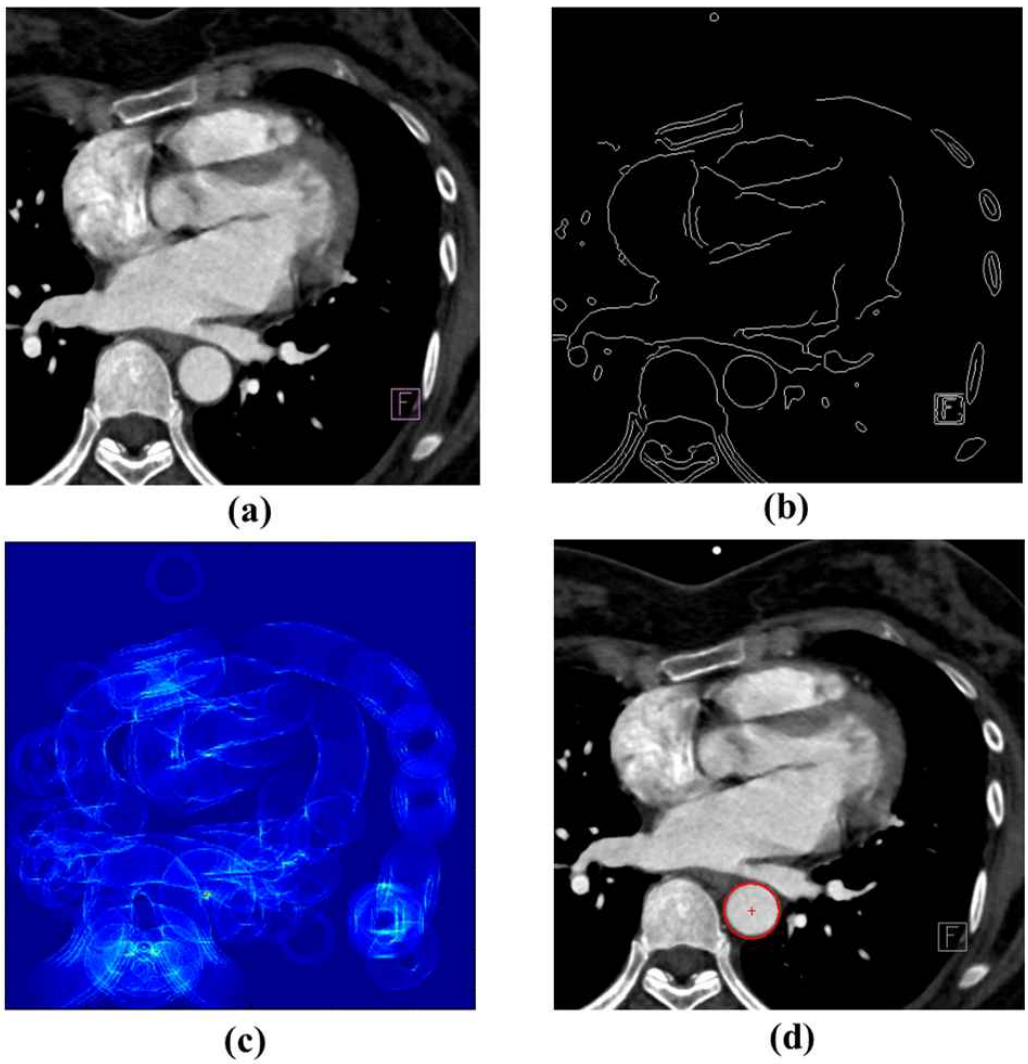

Figure 5.3 Aorta detection using circular Hough transform in MDCT image (a) cardiac MDCT (b) edge detection (c) accumulation array from CHT (d) aorta segmentation result

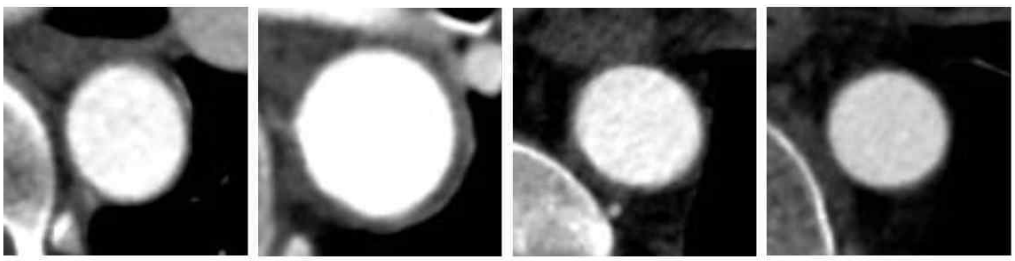

Figure 5.4 Sample images of extracted aorta from MDCT image

5.2. Estimation of Aortic Wall

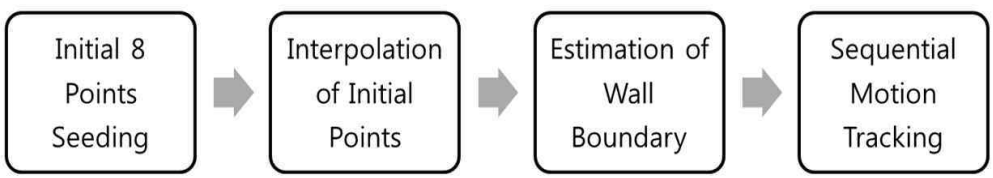

Figure 5.5 Flow chart of aorta wall point tracking method in MDCT and MR image

Seed points of aorta boundary are the starting points for segmentation of wall boundary and its selection is very important for the wall motion tracking. If a seed point is selected outside the target blood vessel, the final motion tracking result would be definitely incorrect. In order to make the correct segmentation of boundary and reduce workload in image process, it is necessary to develop semi-automatic wall motion tracking method. Figure 5.5 shows the flow chart of aorta wall point tracking method in MDCT and MR images.

5.2.1. Selection of Initial Points of Aortic Wall

The initial points of wall border is visually identified by the user and manually obtained. The eight initial points were manually marked along the wall border clockwise direction from the top. The angle between each point was about 45 degree. The lumen interface of the aorta wall was manually marked in MDCT and MR image. Figure 5.6 shows the initial pointing of aorta boundary.

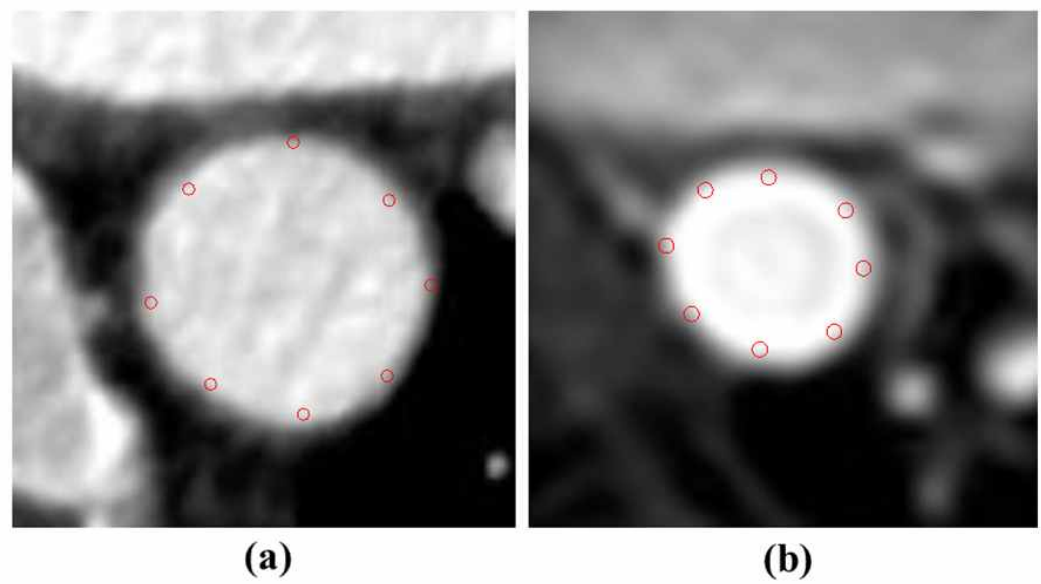

Figure 5.6 Initial pointing of wall boundary (A) aorta in MDCT image (b) aorta in MR image

5.2.2. Estimation of Wall Boundary

In this section, estimation of aorta boundary in MDCT and MR is introduced. Aorta image by MDCT and MR has enhanced contrast properties due to the image acquisition method. Figure 5.7 represents the candidate points of aorta boundary and each line profiles. It shows the high pixel value of aorta area. The goal of this step is to refined aortic boundary points decision from initial mark. The proposed method has two main steps. Firstly, the initial points are increased using linear interpolation. As a result, the number of wall boundary candidate point becomes 48. Although the method creates the initial boundary, the shape does not fit on the desirable wall boundary due to the interpolation method. Secondly, each boundary candidate points were investigated through the lines which pass the initial points including interpolated points. The range of profiles starts from the inner aorta to 70 % position of the aorta radius.

Figure 5.7 shows intensity profiles of aorta in MDCT. Figure 5.7 (a) represents aorta boundary candidate interpolation and the lines of each point in MDCT image. Figure 5.7 (b) shows the pixel values of each line. Figure 5.8 shows the wall boundary finding process and the result of aorta boundary extraction. Figure 5.8 (a) Red color ‘+’ mark represent the center of aorta and black color ‘o’ marks are the candidate wall boundary points before the refined (b) It shows the aorta boundary extraction result in MDCT aorta image.

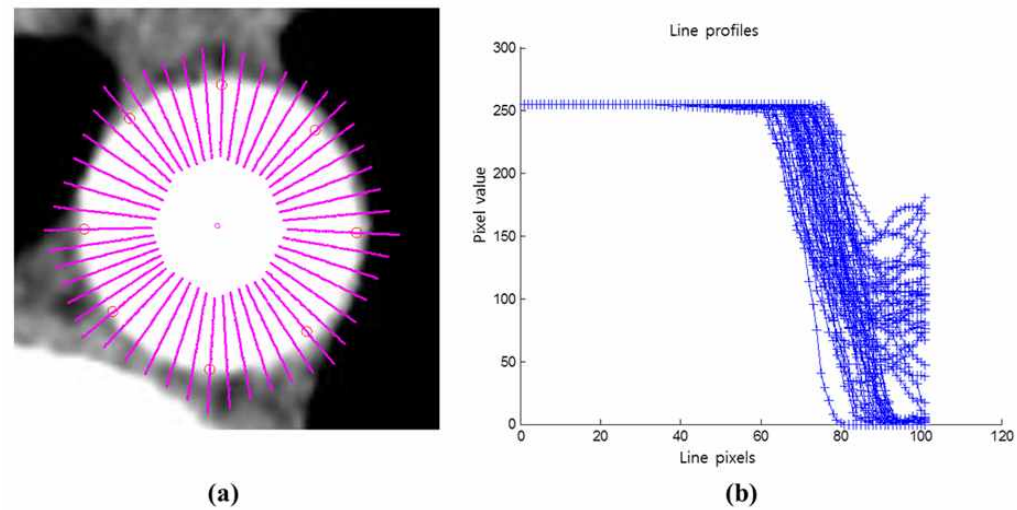

Figure 5.7 Intensity profiles of aorta in MDCT (a) represents aorta boundary candidate interpolation and the lines of each point in MDCT image. (b) shows the pixel values of each line

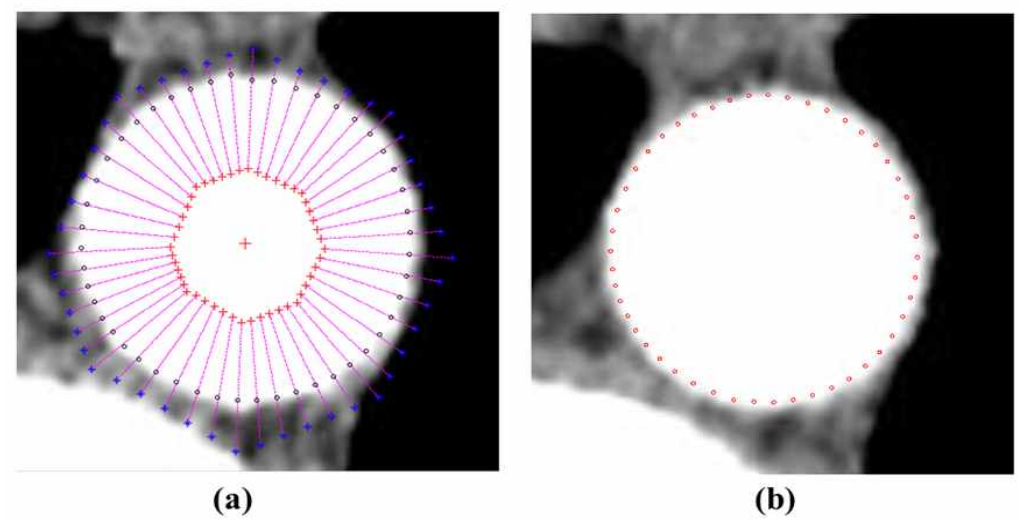

Figure 5.8 Wall boundary extraction on first frame (a) Red color '+' mark represent the center of aorta and black color 'o' marks are the candidate wall boundary points before the refined (b) It shows the aorta boundary extraction result in MDCT aorta image

5.2.3. Sequential Tracing from the Initial Image Frame

The manual placement of target blood vessel boundary tracing over 1 frame is then automatically tracked throughout the image frames. Figure 5.9 shows the process of wall boundary tracking along the image sequences.

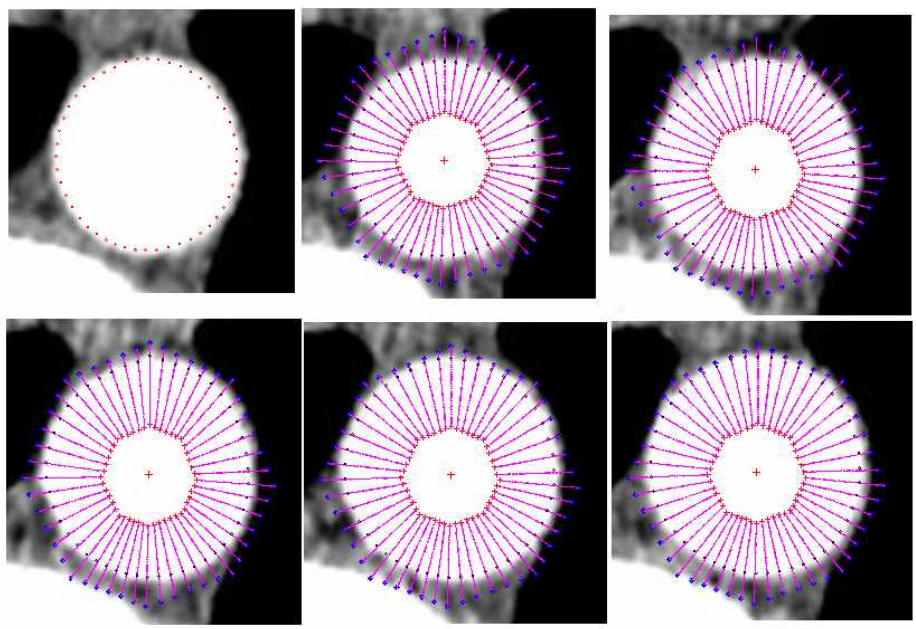

Figure 5.9 The selected result image frames 1 to 6 of aorta boundary extraction in MDCT image

5.3. Analysis of Aortic Motion

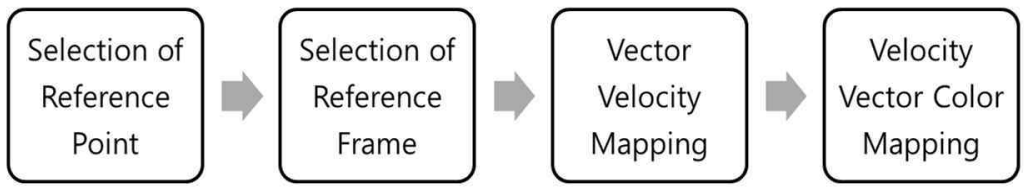

Figure 5.10 The flowchart for velocity vector mapping

This section explains the description of method for vascular wall motion movement and motion analysis. The visualization of movement in the sequential images provides a quantitative source of their motion in space.

The position of an object is given by the displacement vector that locates an object relative to origin. Velocity is a vector quantity that refers to the rate at which an object changes its position from the origin.

The wall motion in the image could be represented by a 2-D vector field V(x,y,t) that specifies the direction and magnitude of velocity at points with coordinates (x,y) at specific time t.

5.3.1. Factors for Aortic Wall Motion Visualization

This dissertation investigated the cross-sectional image of aorta and have interested in aortic motion analysis.

As a result, the position information of estimated wall points and the center point of blood vessel was extracted throughout image frames. It is a result from previous wall point tracking. The points will be arrays.

The center point is also can be a reference point of wall boundary points. The radius is calculated on the basis of average between center point and each 48 wall boundary points. This investigation was performed to find the frame when blood vessel contraction. The movements of wall boundary points are plotted as shown Figure 5.11.

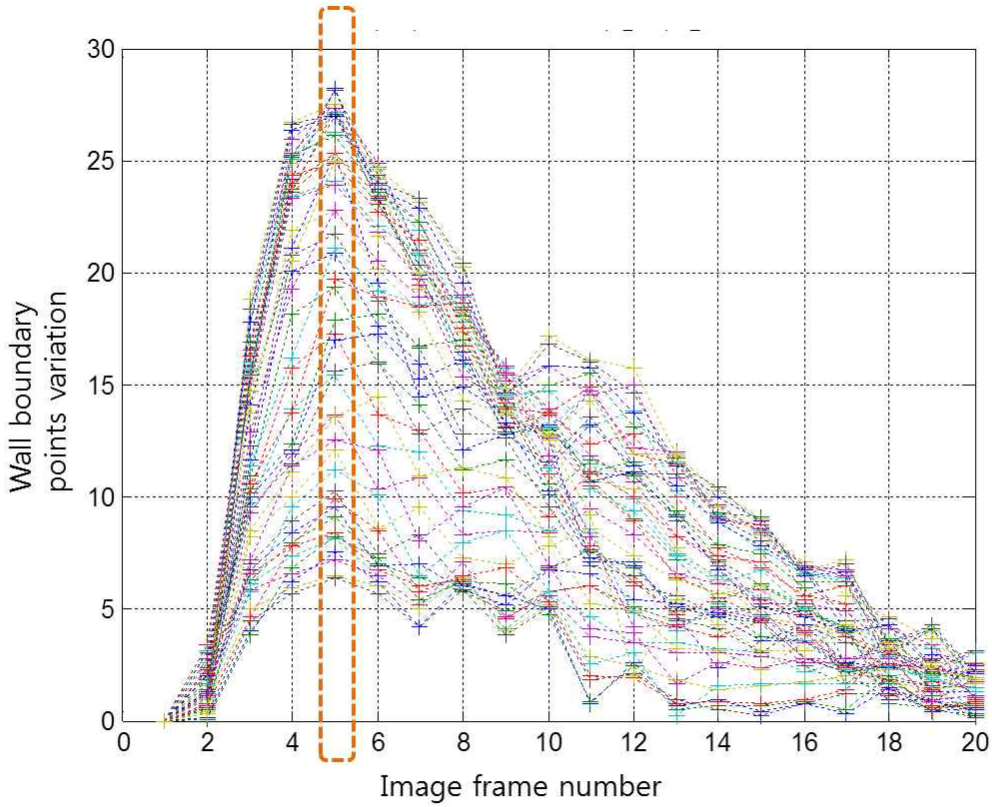

Figure 5.11 Wall movement throughout image frames. The orange color dotted box means the frame when blood vessel expansion

5.3.2. Definition of Reference Point

In order to visualize the blood vessel wall motion, it is important to define the point of viewing reference. The wall points were moving with respect to the center of blood vessel. The center was extracted from intersections of 48 modified aortic wall points. It also has variations in each frame. Figure 5.12 shows the pixel movement of center point. It had variations with wide rage on other data set. The center point position had to be updated to hold the proper viewing reference. Figure 5.12 (a) shows the graph of pixel variation along the image sequence, figure 5.12 (b) represent the average and standard deviation of center point variation and figure 5.12 (c) shows the center moves along the image sequence in image domain.

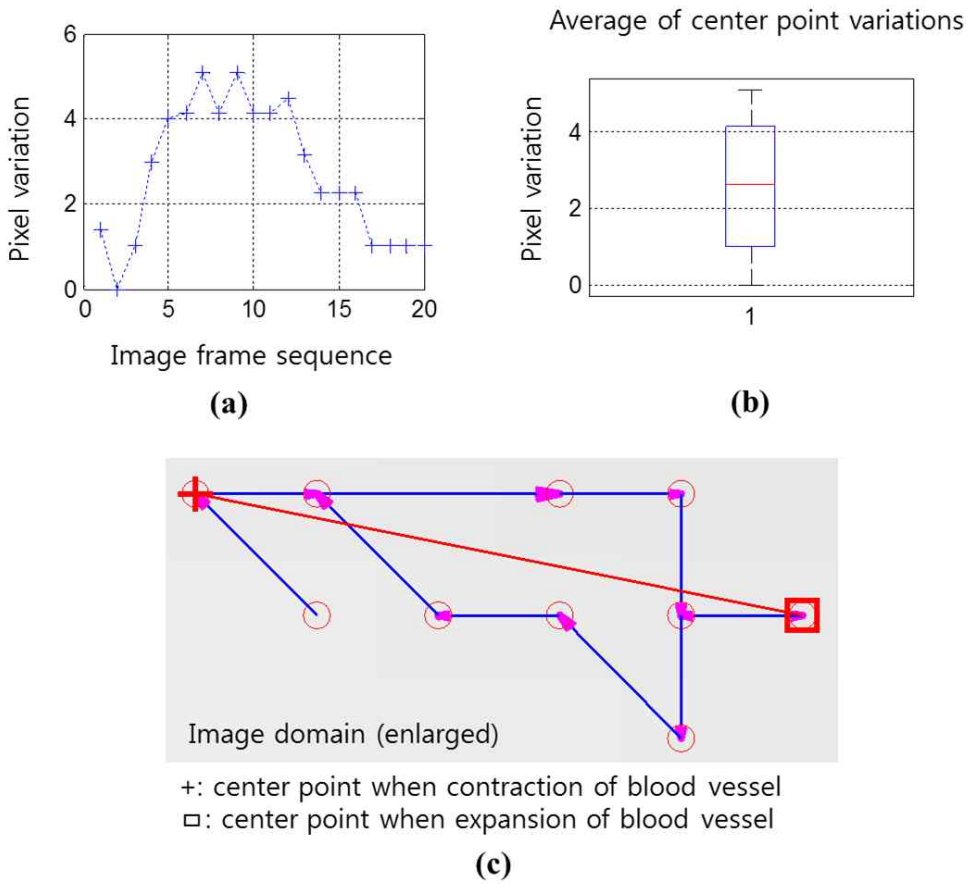

Figure 5.12 Aortic centroid variations (a) graph of pixel variation along the image sequence (b) average and standard deviation of center point variation (c) center moves along the image sequence in image domain

5.3.3. Aortic Wall Motion Visualization

The velocity vector mapping provides the displacement of wall boundary points, and the velocity. Figure 5.13 shows the result of vector velocity mapping. The red circles on the image represent the aorta boundary point when contraction and the black circles mean extended position of boundary. The distance between the two circles shows velocity or strain of blood vessel wall. The red cross of the image means the center of vascular when contraction. While the blue circle indicate the center in current image frame.

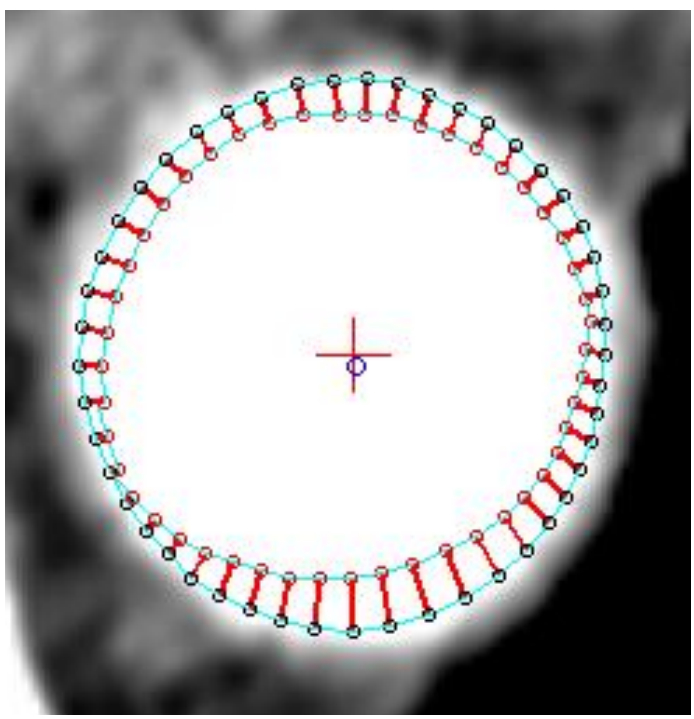

Figure 5.13 Vector velocities mapping of aorta wall point movement in MDCT image

5.3.4. Wall Movement Velocity Mapping in Color

The velocity could be described as a length of two wall indicated points. However, the difference of velocity in each point is not intuitive. The method for velocity mapping in color was introduced in this chapter. Figure 5.14 (a) is accumulative trace of wall point's movement from point number 1 to the final point number 48. The mean value of the movement and investigated as shown in Figure 5.14 (b) and (c). In practice, the velocities were classified into three categories. Finally, the color assigned vector velocity mapping was completed as shown in Figure 5.15. The color red represented the upper class, green stands for middle class and blue depicted lower class of wall motion of points.

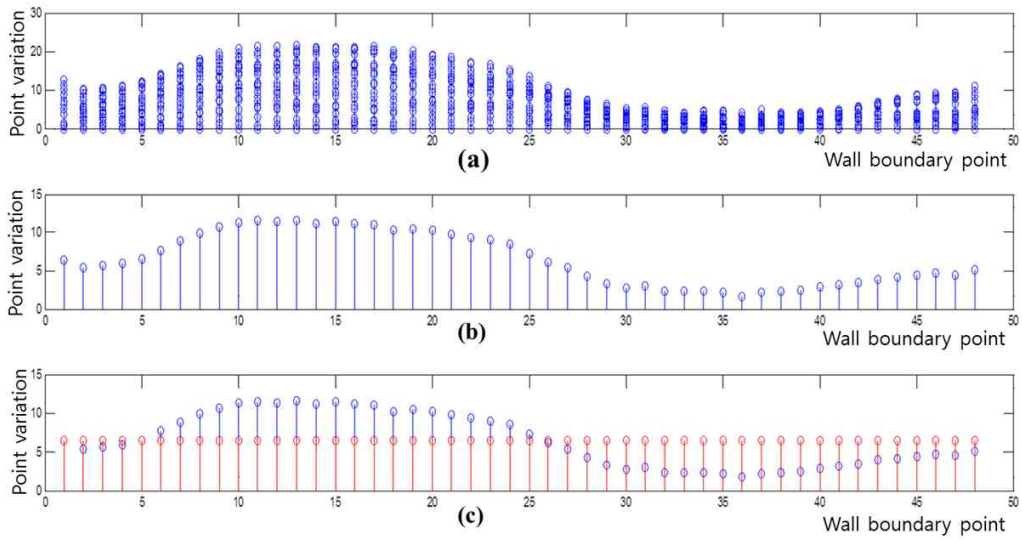

Figure 5.14 Wall point variation (a) The accumulative trace of wall motion movement at each point (b) averaged value of point variation at each point (c) red pole stands for the mean value of point variation, blue pole comes from graph

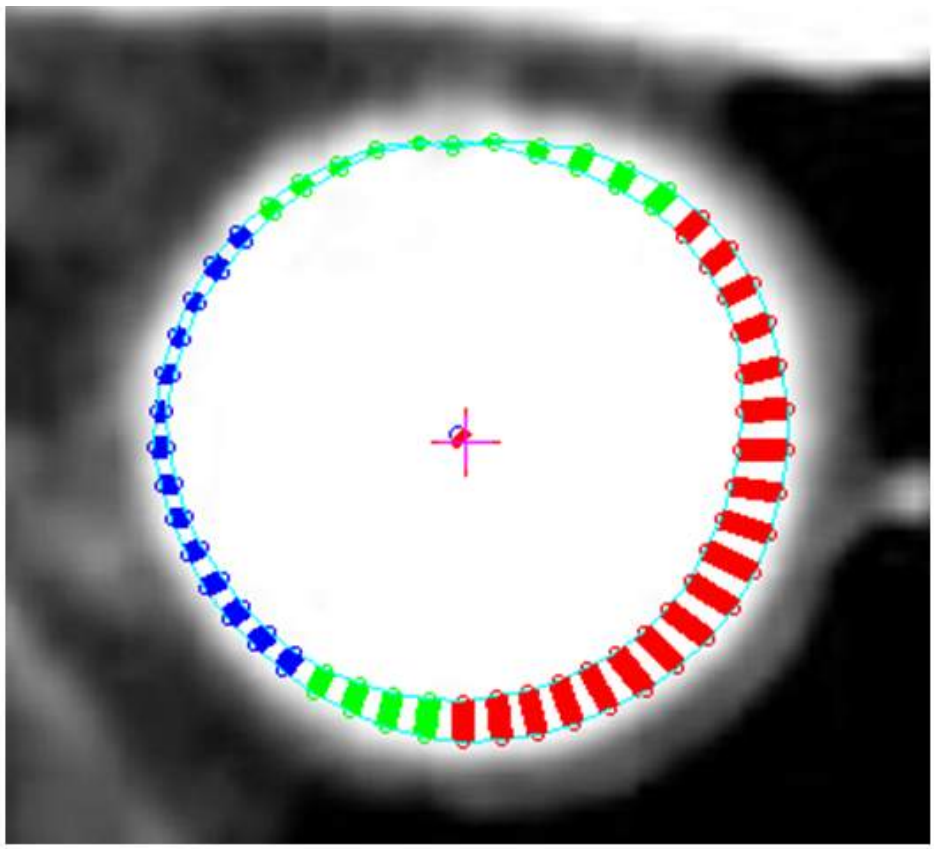

Figure 5.15 Mapping of clustered vector velocities. Each color shows the velocity class; red for upper, green for middle and blue for lower class of motion

5.3.5. Aortic Displacement

In this section, display of aortic displacement in MDCT and Cine-MR is introduced. The aorta motion was classified into two; wall movement and aortic displacement. In order to visualize the aortic displacement, it is important to define the centroid of aorta. The aorta were moving with respect to the center of blood vessel. The centroid was extracted from intersections of 48 aorta wall points. It also has variations in each frame.

Figure 5.16 shows the example of aortic displacement magnitude and direction in each position. The centroid had to be updated to hold the proper aorta place. The intersection of quadrant was the reference point of the aortic displacement. The vector means the aorta motion direction and magnitude. It shows the aorta moved along the time in image domain.

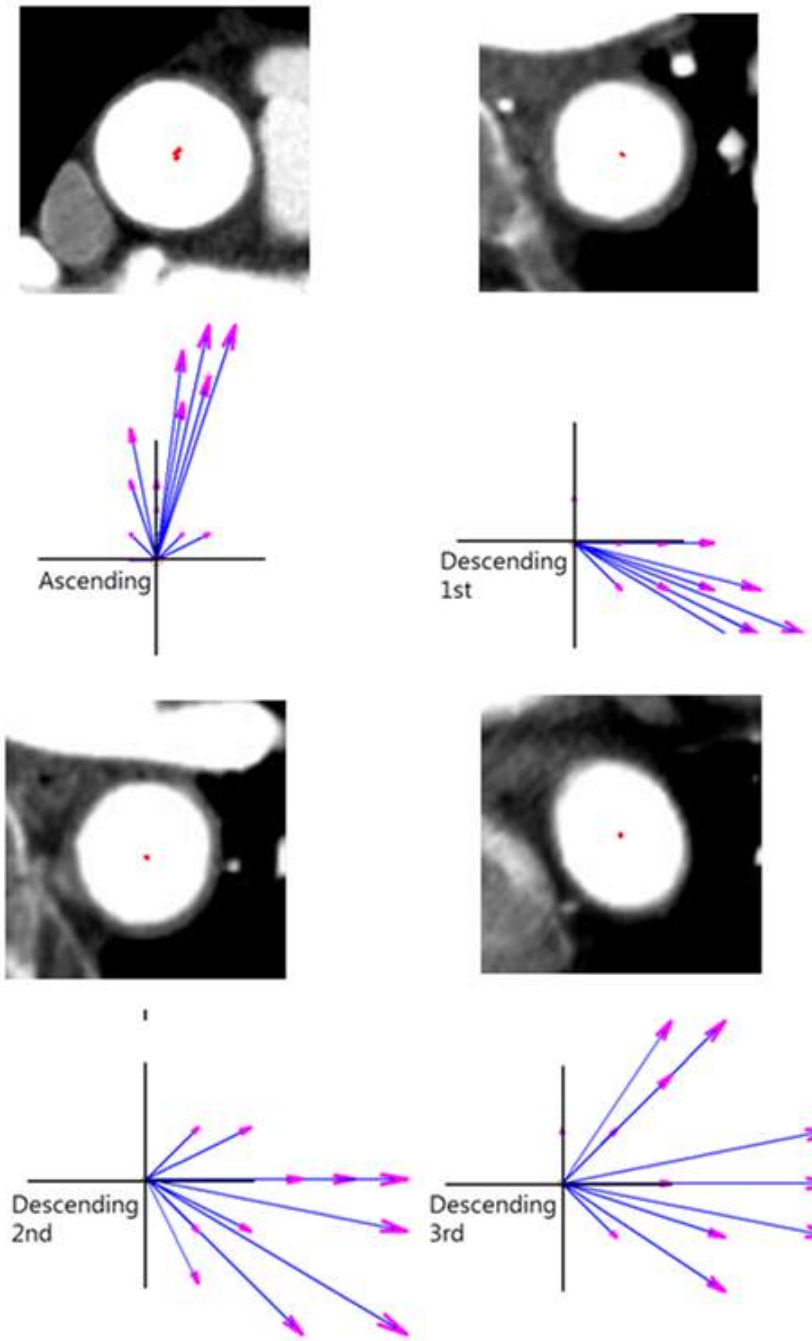

Figure 5.16 Example of aortic displacement magnitude and direction in each position

5.4. Discussion

In this chapter, a new visualization method for dynamic aorta motion and property were proposed. Aorta motion was evaluated by semi-automatic segmentation of the aortic lumen and calculation of the wall movement including aorta displacement.

As s first step for aortic mechanical and hemodynamic characterizations, segmentation of the aortic lumen is essential for the accurate estimation of the clinical parameters. However, the superior temporal resolution increases the number of cardiac phases to be segmented, making the manual delineation of the aorta of the aortic lumen complex and time consuming. Also, PC modulus image intensity variations over the cardiac cycle caused by the increase in flow velocities can create inaccuracies in the contour location, resulting in a difficult detection of small variations in lumen area.

Chapter 6

6. Clinical Validation

In this chapter, the clinical validation of aorta motion assessment using MDCT and Cine-MR images are presented. This chapter is consists of two sections. Section 6.1 ‘Aorta Motion Assessment using MDCT images’ describes the method for aortic motion property analysis and depiction graph of aorta calcification. Section 6.2 ‘Aorta Motion Assessment using Cine-MR images’ introduces the aortic motion property in Turner syndrome.

6.1. Aorta Motion Assessment using MDCT Images

6.1.1. Subject and Image Data

The aorta images of 30 subjects (14 men, 16 women; mean age, 55.9 ± 14.99 years; range, 31-80 years) who underwent heart scanning during period April 2010 to October 2011 at Severance hospital were recruited in this study. The MDCT data of all subjects were collected during 18 month.

They have valvular heart disease.

All images from MDCT were reviewed and sampled by radiologist using Syngo CT (Siemens, German). Retrospectively gated MDCT images were provided to analysis. Table 6.1 shows the clinical characteristics of the subjects and acquired image data.

Table 6.1 Subjects and MDCT image data of study population

Group	Subject No.	Age	Sex	BPM	Position	Frame	Pixel Spacing (mm)
1	1	49	M	62	1st	20	0.39
					2nd	20	
					3rd	20	
1	2	66	M	56	1st	20	0.38
					2nd	20	
					3rd	20	
1	3	80	F	67	1st	20	0.44
					2nd	20	
					3rd	20	
2	4	49	M	46	1st	20	0.36
					2nd	20	
					3rd	20	
2	5	47	F	59	1st	20	0.41
					2nd	20	
					3rd	20	
2	6	51	F	67	1st	20	0.37
					2nd	20	
					3rd	20	
2	7	31	F	60	1st	20	0.38
					2nd	20	
					3rd	20	
2	8	54	M	54	1st	20	0.44
					2nd	20	
					3rd	20	
3	9	44	F	48	1st	20	0.41
					2nd	20	
					3rd	20	

3	10	78	M	84	1st	20	0.41
					2nd	20	
					3rd	20	
3	11	40	F	62	1st	20	0.33
					2nd	20	
					3rd	20	
3	12	69	M	60	1st	20	0.4
					2nd	20	
					3rd	20	
3	13	72	F	59	1st	20	0.38
					2nd	20	
					3rd	10	
3	14	55	F	40	1st	20	0.41
					2nd	20	
					3rd	20	
3	15	62	F	66	1st	20	0.31
					2nd	20	
					3rd	20	
3	16	50	M	45	1st	20	0.42
					2nd	20	
					3rd	20	
3	17	54	M	71	1st	20	0.44
					2nd	20	
					3rd	20	
3	18	72	F	61	1st	20	0.42
					2nd	20	
					3rd	20	
3	19	77	M	65	1st	20	0.38
					2nd	20	
					3rd	20	
4	20	37	F	54	1st	20	0.3
					2nd	20	
					3rd	20	
4	21	33	M	86	1st	20	0.37
					2nd	20	
					3rd	20	
4	22	37	F	62	1st	20	0.35
					2nd	20	
					3rd	20	

4	23	36	F	76	1st	19	0.32
					2nd	19	
					3rd	8	
5	24	59	M	53	1st	10	0.16
					2nd	10	
					3rd	10	
5	25	72	F	58	1st	8	0.22
					2nd	10	
					3rd	10	
5	26	79	F	74	1st	10	0.2
					2nd	10	
					3rd	10	
5	27	48	M	35	1st	11	0.18
					2nd	11	
					3rd	11	
5	28	66	F	59	1st	10	0.17
					2nd	10	
					3rd	10	
5	29	68	M	43	1st	10	0.19
					2nd	10	
					3rd	10	
5	30	43	M	61	1st	10	0.16
					2nd	10	
					3rd	10	

6.1.2. Aortic Wall Movement in MDCT Images

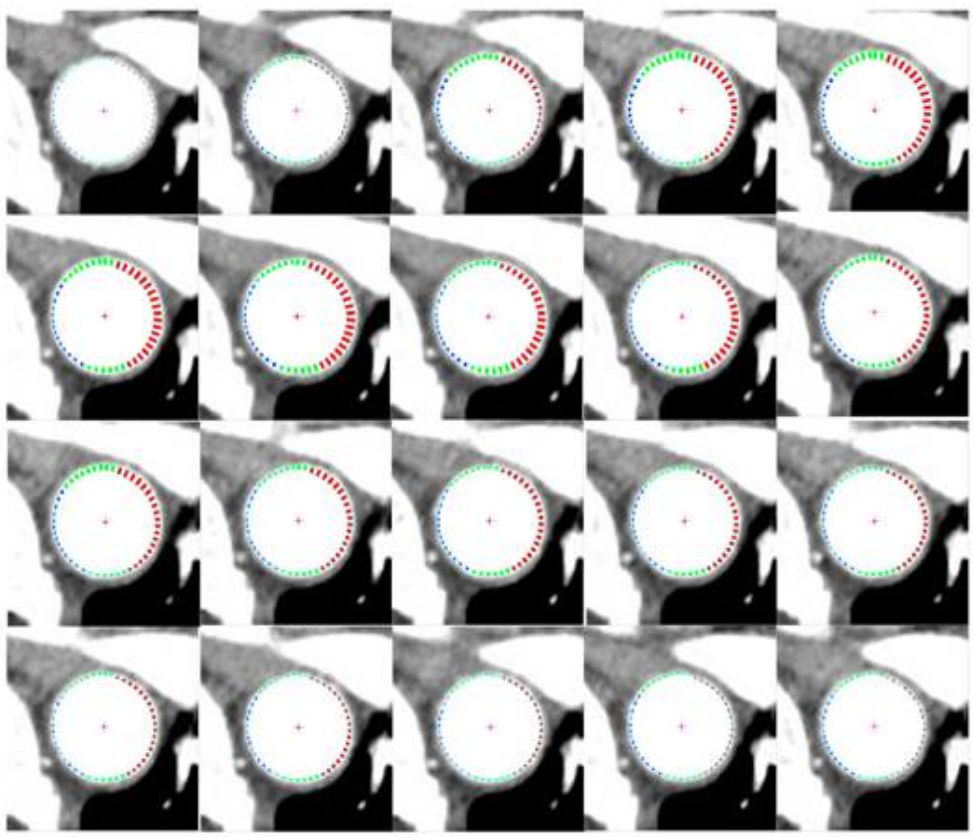

Figure 6.1 Example of phase MDCT images after mapping of vector velocity

In this section, the wall movement distance of descending aorta using MDCT images were calculated and depicted. To demonstrated this outcome, descending aorta boundary segmentation and wall motion tracking were performed. Figure 6.1 shows the results of wall motion tracking by

proposed algorithms. The magnitude of wall movement velocity throughout the cardiac cycle was obtained. The point velocity was classified into three groups; red, green, blue. The colors were assigned by wall movement distance in order. The red clustered point means the fastest variation among the three groups. The green and blue represented the second and third group. Figure 6.2 shows example of wall movement profiles. Figure 6.2 (a) represents the every 48 wall points variations and 6.2 (b) shows the clustered points graph by vector velocity. The dashed red line with cross represented the fastest wall motion cluster. The dashed magenta line with circle and dashed blue line with cross was the second and the third cluster, respectively in figure 6.2 (b). The y-axis value of clustered points variation represents the mean variation in each frame. In figure 6.2 (b), the orange rectangular means the frame of aorta expansion. It corresponds with figure 6.2 (c).

The wall movement of descending aorta for total subjects were presented as mean ± standard deviation (S.D.) as shown in Table 6.2.

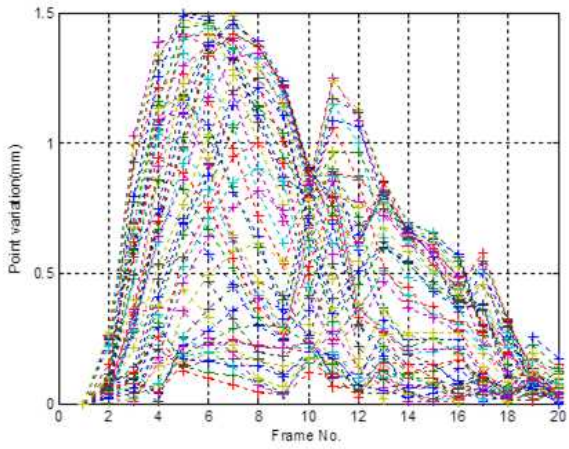

(a)

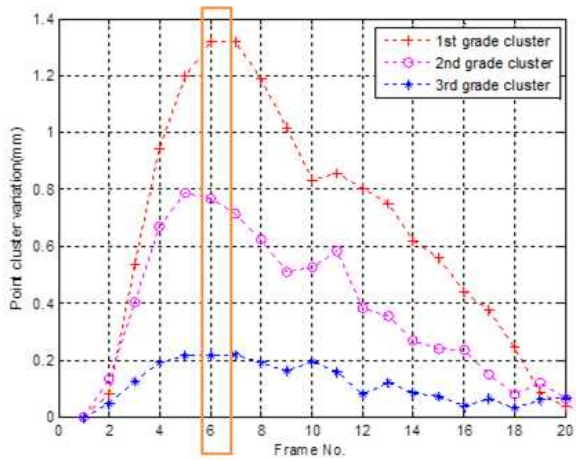

(b)

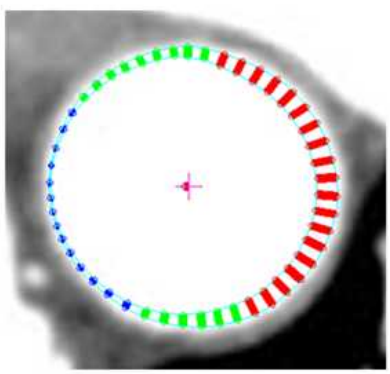

(c)

Figure 6.2 Example of aorta wall movement profiles at the 2nd position of descending aorta (a) aorta wall variation graph (b) movement of clustered by velocity (c) vector velocity mapping when descending aorta expansion

Table 6.2 Subjects and wall movement of descending aorta

Subject No.	Age	Frame	Position	Point Movement Average (mm)			
				All	First	Second	Third
				Mean ± SD	Mean ± SD	Mean ± SD	Mean ± SD
1	49	20	1st	0.48 ± 0.21	0.68 ± 0.36	0.49 ± 0.27	0.21 ± 0.10
		20	2nd	0.46 ± 0.25	0.74 ± 0.39	0.36 ± 0.18	0.19 ± 0.08
		20	3rd	0.35 ± 0.21	0.57 ± 0.34	0.30 ± 0.13	0.11 ± 0.05
2	66	20	1st	0.19 ± 0.06	0.26 ± 0.22	0.19 ± 0.08	0.11 ± 0.04
		20	2nd	0.33 ± 0.17	0.52 ± 0.35	0.28 ± 0.17	0.14 ± 0.07
		20	3rd	0.75 ± 0.55	1.38 ± 0.65	0.45 ± 0.22	0.21 ± 0.09
3	80	20	1st	0.29 ± 0.17	0.44 ± 0.17	0.25 ± 0.12	0.13 ± 0.05
		20	2nd	0.33 ± 0.24	0.59 ± 0.25	0.21 ± 0.11	0.09 ± 0.07
		20	3rd	0.26 ± 0.18	0.44 ± 0.24	0.18 ± 0.08	0.11 ± 0.04
4	49	20	1st	0.51 ± 0.26	0.80 ± 0.46	0.43 ± 0.25	0.21 ± 0.10
		20	2nd	0.56 ± 0.24	0.80 ± 0.59	0.56 ± 0.39	0.24 ± 0.18
		20	3rd	0.69 ± 0.49	1.24 ± 0.90	0.47 ± 0.33	0.18 ± 0.13
5	47	20	1st	0.58 ± 0.26	0.86 ± 0.60	0.55 ± 0.35	0.25 ± 0.14
		20	2nd	0.58 ± 0.27	0.86 ± 0.53	0.55 ± 0.40	0.24 ± 0.14
		20	3rd	0.56 ± 0.37	0.96 ± 0.66	0.44 ± 0.27	0.15 ± 0.08
6	51	20	1st	0.66 ± 0.44	1.15 ± 0.63	0.46 ± 0.19	0.22 ± 0.08
		20	2nd	0.62 ± 0.36	1.01 ± 0.61	0.52 ± 0.27	0.20 ± 0.10
		20	3rd	0.52 ± 0.18	0.69 ± 0.42	0.53 ± 0.34	0.27 ± 0.14

7	31	20	1st	0.51 ± 0.33	0.86 ± 0.65	0.39 ± 0.21	0.16 ± 0.08
		20	2nd	0.61 ± 0.35	0.99 ± 0.77	0.48 ± 0.27	0.22 ± 0.15
		20	3rd	0.66 ± 0.41	1.09 ± 0.64	0.58 ± 0.35	0.16 ± 0.06
8	54	20	1st	0.53 ± 0.22	0.74 ± 0.44	0.50 ± 0.32	0.28 ± 0.14
		20	2nd	0.66 ± 0.39	1.08 ± 0.57	0.55 ± 0.26	0.20 ± 0.07
		20	3rd	0.56 ± 0.26	0.83 ± 0.60	0.50 ± 0.30	0.27 ± 0.12
9	44	20	1st	0.48 ± 0.08	0.56 ± 0.35	0.47 ± 0.32	0.37 ± 0.23
		20	2nd	0.43 ± 0.17	0.61 ± 0.33	0.40 ± 0.23	0.22 ± 0.15
		20	3rd	0.29 ± 0.19	0.49 ± 0.33	0.24 ± 0.12	0.07 ± 0.04
10	78	20	1st	0.21 ± 0.11	0.33 ± 0.18	0.18 ± 0.09	0.09 ± 0.04
		20	2nd	0.22 ± 0.08	0.30 ± 0.16	0.20 ± 0.09	0.12 ± 0.06
		20	3rd	0.29 ± 0.21	0.46 ± 0.23	0.23 ± 0.10	0.12 ± 0.07
11	40	20	1st	0.61 ± 0.34	0.97 ± 0.67	0.51 ± 0.22	0.22 ± 0.12
		20	2nd	0.86 ± 0.50	1.41 ± 0.74	0.62 ± 0.23	0.36 ± 0.14
		20	3rd	0.88 ± 0.52	1.46 ± 0.81	0.69 ± 0.32	0.31 ± 0.13
12	69	20	1st	0.47 ± 0.27	0.77 ± 0.33	0.37 ± 0.18	0.18 ± 0.07
		20	2nd	0.42 ± 0.27	0.71 ± 0.42	0.32 ± 0.14	0.14 ± 0.06
		20	3rd	0.39 ± 0.28	0.71 ± 0.44	0.28 ± 0.17	0.09 ± 0.04
13	72	20	1st	0.48 ± 0.32	0.84 ± 0.50	0.33 ± 0.16	0.14 ± 0.05
		20	2nd	0.51 ± 0.26	0.78 ± 0.46	0.49 ± 0.26	0.19 ± 0.09
		10	3rd	0.53 ± 0.35	0.92 ± 0.48	0.40 ± 0.19	0.14 ± 0.06

14	55	20	1st	0.65 ± 0.41	1.10 ± 0.68	0.50 ± 0.28	0.20 ± 0.10
		20	2nd	0.59 ± 0.25	0.85 ± 0.57	0.57 ± 0.34	0.30 ± 0.17
		20	3rd	0.57 ± 0.27	0.85 ± 0.54	0.54 ± 0.26	0.24 ± 0.11
15	62	20	1st	0.40 ± 0.13	0.51 ± 0.26	0.42 ± 0.22	0.23 ± 0.12
		20	2nd	0.52 ± 0.26	0.80 ± 0.35	0.44 ± 0.15	0.22 ± 0.07
		20	3rd	0.24 ± 0.12	0.36 ± 0.23	0.21 ± 0.11	0.10 ± 0.04
16	50	20	1st	0.52 ± 0.33	0.86 ± 0.61	0.46 ± 0.28	0.13 ± 0.06
		20	2nd	0.59 ± 0.31	0.92 ± 0.44	0.48 ± 0.32	0.27 ± 0.17
		20	3rd	0.79 ± 0.48	1.34 ± 0.63	0.56 ± 0.21	0.31 ± 0.12
17	54	20	1st	0.66 ± 0.44	1.16 ± 0.65	0.48 ± 0.23	0.20 ± 0.08
		20	2nd	0.65 ± 0.38	1.08 ± 0.68	0.49 ± 0.21	0.24 ± 0.12
		20	3rd	0.58 ± 0.36	0.95 ± 0.73	0.52 ± 0.31	0.13 ± 0.05
18	72	20	1st	0.21 ± 0.09	0.31 ± 0.18	0.18 ± 0.10	0.11 ± 0.05
		20	2nd	0.42 ± 0.23	0.65 ± 0.35	0.39 ± 0.22	0.13 ± 0.06
		20	3rd	0.29 ± 0.18	0.47 ± 0.27	0.24 ± 0.14	0.09 ± 0.04
19	77	20	1st	0.54 ± 0.25	0.79 ± 0.49	0.50 ± 0.33	0.22 ± 0.12
		20	2nd	0.57 ± 0.23	0.78 ± 0.57	0.58 ± 0.26	0.29 ± 0.13
		20	3rd	0.44 ± 0.26	0.70 ± 0.59	0.38 ± 0.16	0.15 ± 0.09
20	37	20	1st	0.64 ± 0.50	1.22 ± 0.75	0.39 ± 0.22	0.13 ± 0.06
		20	2nd	0.55 ± 0.34	0.92 ± 0.67	0.41 ± 0.25	0.19 ± 0.11
		20	3rd	0.49 ± 0.18	0.66 ± 0.47	0.49 ± 0.33	0.25 ± 0.11

21	33	20	1st	0.74 ± 0.49	1.26 ± 0.73	0.55 ± 0.30	0.24 ± 0.11
		20	2nd	0.67 ± 0.36	1.05 ± 0.60	0.59 ± 0.30	0.25 ± 0.12
		20	3rd	0.53 ± 0.33	0.88 ± 0.67	0.43 ± 0.23	0.18 ± 0.07
22	37	20	1st	0.51 ± 0.18	0.68 ± 0.41	0.52 ± 0.31	0.27 ± 0.18
		20	2nd	0.41 ± 0.24	0.66 ± 0.43	0.38 ± 0.25	0.12 ± 0.07
		20	3rd	0.51 ± 0.25	0.76 ± 0.54	0.50 ± 0.30	0.18 ± 0.10
23	36	19	1st	0.57 ± 0.39	1.00 ± 0.57	0.39 ± 0.20	0.17 ± 0.09
		19	2nd	0.47 ± 0.23	0.69 ± 0.34	0.46 ± 0.22	0.18 ± 0.08
		8	3rd	0.40 ± 0.29	0.73 ± 0.60	0.26 ± 0.17	0.11 ± 0.07
24	59	10	1st	0.21 ± 0.12	0.34 ± 0.23	0.18 ± 0.10	0.08 ± 0.04
		10	2nd	0.16 ± 0.08	0.25 ± 0.15	0.12 ± 0.07	0.07 ± 0.04
		10	3rd	0.18 ± 0.08	0.25 ± 0.22	0.15 ± 0.11	0.10 ± 0.05
25	72	8	1st	0.11 ± 0.06	0.18 ± 0.13	0.09 ± 0.06	0.05 ± 0.03
		10	2nd	0.17 ± 0.09	0.27 ± 0.15	0.16 ± 0.07	0.07 ± 0.03
		10	3rd	0.18 ± 0.11	0.30 ± 0.17	0.15 ± 0.09	0.06 ± 0.02
26	79	10	1st	0.08 ± 0.05	0.14 ± 0.07	0.05 ± 0.02	0.03 ± 0.01
		10	2nd	0.10 ± 0.03	0.13 ± 0.07	0.10 ± 0.05	0.06 ± 0.02
		10	3rd	0.14 ± 0.06	0.21 ± 0.14	0.12 ± 0.06	0.07 ± 0.03
27	48	11	1st	0.20 ± 0.12	0.33 ± 0.27	0.16 ± 0.14	0.06 ± 0.04
		11	2nd	0.14 ± 0.06	0.19 ± 0.14	0.15 ± 0.09	0.07 ± 0.04
		11	3rd	0.17 ± 0.10	0.26 ± 0.18	0.15 ± 0.10	0.05 ± 0.03

28	66	10	1st	0.15 ± 0.05	0.20 ± 0.15	0.15 ± 0.09	0.09 ± 0.05
		10	2nd	0.16 ± 0.09	0.26 ± 0.19	0.12 ± 1.00	0.08 ± 0.04
		10	3rd	0.23 ± 0.14	0.37 ± 0.25	0.18 ± 0.12	0.09 ± 0.05
29	68	10	1st	0.16 ± 0.08	0.24 ± 0.13	0.15 ± 0.08	0.06 ± 0.28
		10	2nd	0.11 ± 0.04	0.15 ± 0.10	0.10 ± 0.07	0.06 ± 0.04
		10	3rd	0.08 ± 0.04	0.12 ± 0.11	0.07 ± 0.04	0.04 ± 0.02
30	43	10	1st	0.32 ± 0.23	0.58 ± 0.33	0.20 ± 0.09	0.10 ± 0.04
		10	2nd	0.30 ± 0.19	0.50 ± 0.36	0.23 ± 0.10	0.09 ± 0.05
		10	3rd	0.25 ± 0.12	0.37 ± 0.31	0.23 ± 0.14	0.11 ± 0.07

6.1.3. Aortic Wall Movement Profiles in Aorta Calcification

Figure 6.3 shows the wall motion profiles and vector velocity when aorta expansion. The orange arrows show the calcium detected on aorta in each image. Figure 6.3 (a) represents wall motion characteristics of subject No. 3 at the 3rd position and figure 6.3 (b) shows the aorta motion of subject No. 26 at the 1st position. The variations of calcification sites were lower than other non-calcification sites. The shapes of points variation profile indicate dyssynchoronous aorta expansion. The clusters which are include the calcification point showed extremely low variation throughout the image samples.

As shown in Table 6.4, averaged aortic wall points movement values were lower than subject No. 22 which has no calcification in blood vessel. Figure 6.4 shows the comparison normal and aorta calcification movement. The averaged total point movement of normal aorta was higher than calcification aorta.

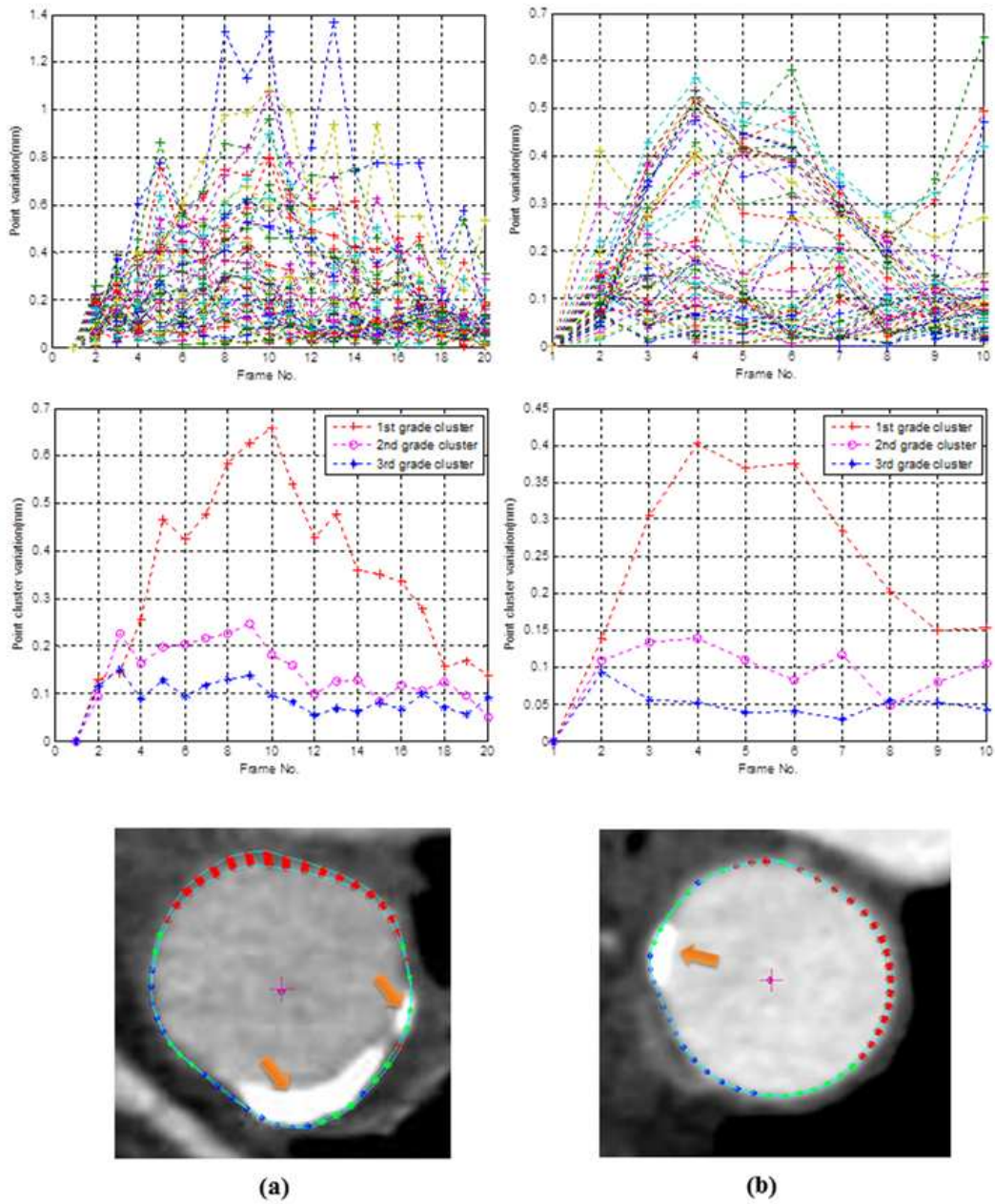

Figure 6.3 Wall motion characteristics in aorta calcification. (Orange arrows mean calcification) (a) subject No. 3 at 3rd position (b) subject No. 26 at 1st position

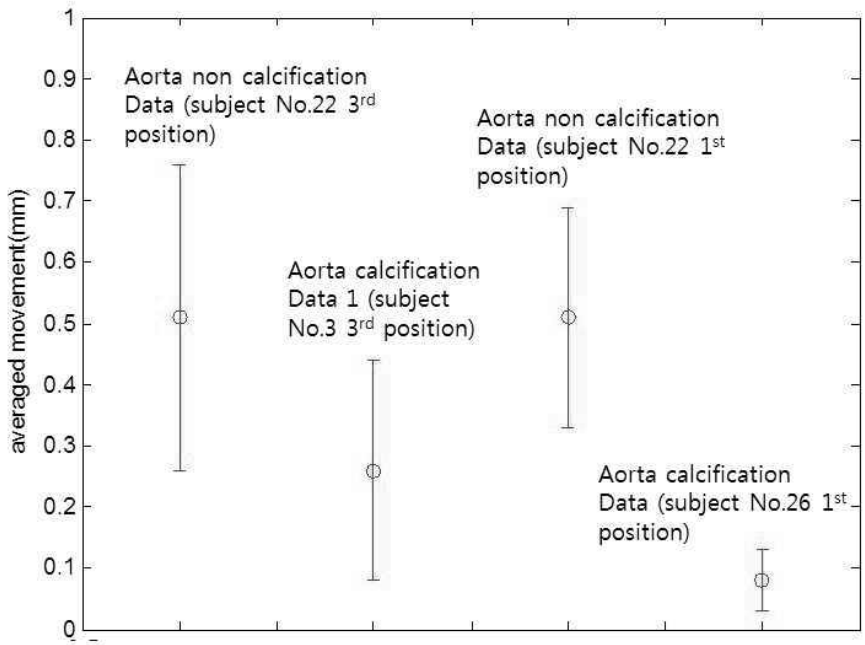

Figure 6.4 Comparison between aorta calcification and normal

6.1.4. Aortic Wall Movement and Age

The scatter plots and Pearson's correlation coefficients of between three different position of descending aorta and ages are illustrated in figure 6.5, 6.6 and 6.7. The averaged wall movement at the 1st position of descending aorta along the entire study population groups in figure 6.5 and the correlation coefficient was -0.63 ($p < 0.001$). Figure 6.6 shows the averaged wall movement at the 2nd position of descending aorta along the entire study population groups and the correlation coefficient was -0.51 ($p < 0.05$). Figure 6.7 represents averaged wall movement at 3rd position of descending aorta along the entire study population groups and the correlation coefficient was -0.45 ($p < 0.05$).

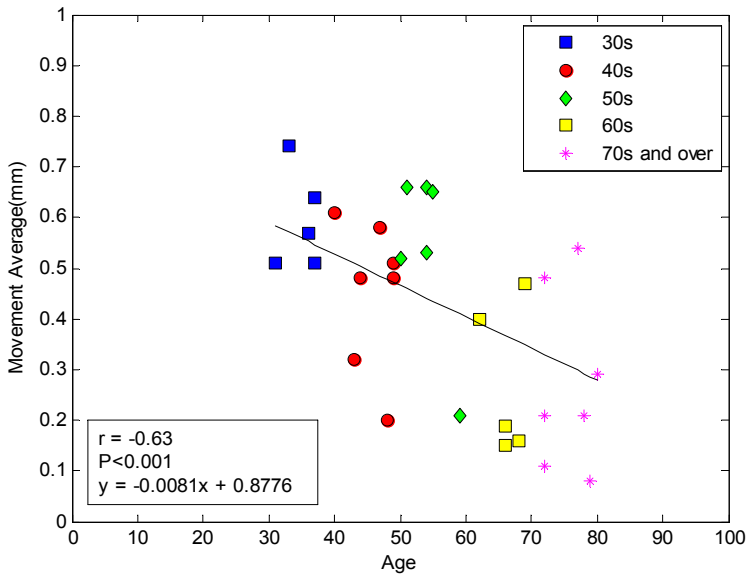

Figure 6.5 Correlation between age and averaged wall movement of thoracic aorta at the 1st position

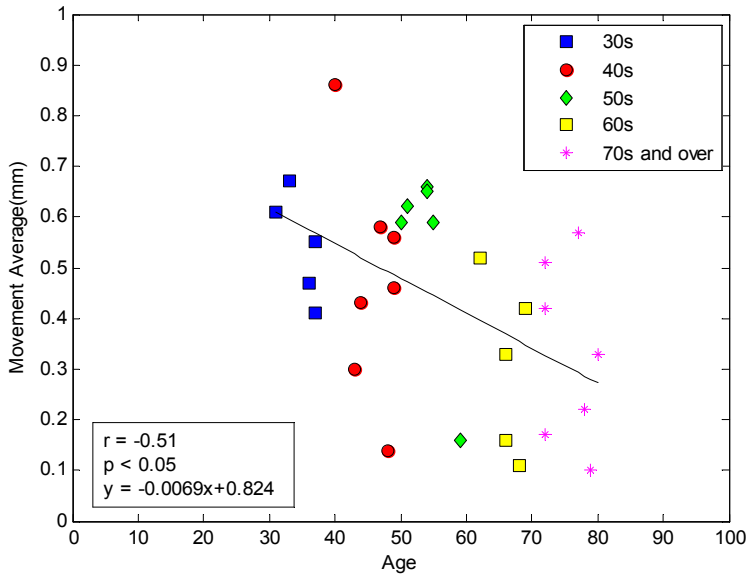

Figure 6.6 Correlation between age and averaged wall movement of thoracic aorta at the 2nd position

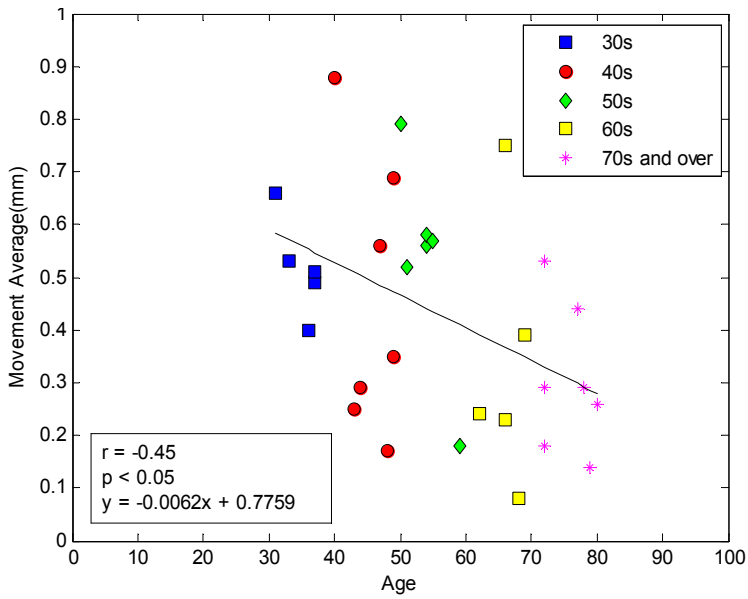

Figure 6.7 Correlation between age and averaged wall movement of thoracic aorta at the 3rd position

6.1.5. Aortic Wall Movement and Position

Table 6.3 represents the relations between age groups and mean of descending aorta wall movement in each position. The wall point movement data are presented as mean ± S.D. There was decrease of the aortic movement at different thoracic levels in age 30s. However, there was not decrease of the aortic movement at different thoracic levels. This tendency doesn't match the fact of thoracic aorta characteristics. According to the research, the elastin ratio is highest in the thoracic part and decreases distally [78]. This difference could be due to the aorta calcification of the investigated population. Figure 6.8 shows boxplot of each thoracic aorta movement distance at their age group.

Table 6.3 Averaged wall movement of descending aorta in each positions and ages

Ages	Averaged wall movement (mm) in each aorta position		
	1st	2nd	3rd
	Mean ± S.D.	Mean ± S.D.	Mean ± S.D.
30s	0.59 ± 0.10	0.54 ± 0.10	0.52 ± 0.09
40s	0.45 ± 0.15	0.48 ± 0.23	0.46 ± 0.26
50s	0.54 ± 0.17	0.55 ± 0.19	0.53 ± 0.20
60s	0.27 ± 0.15	0.31 ± 0.17	0.34 ± 0.26
70s and over	0.27 ± 0.18	0.33 ± 0.18	0.30 ± 0.14

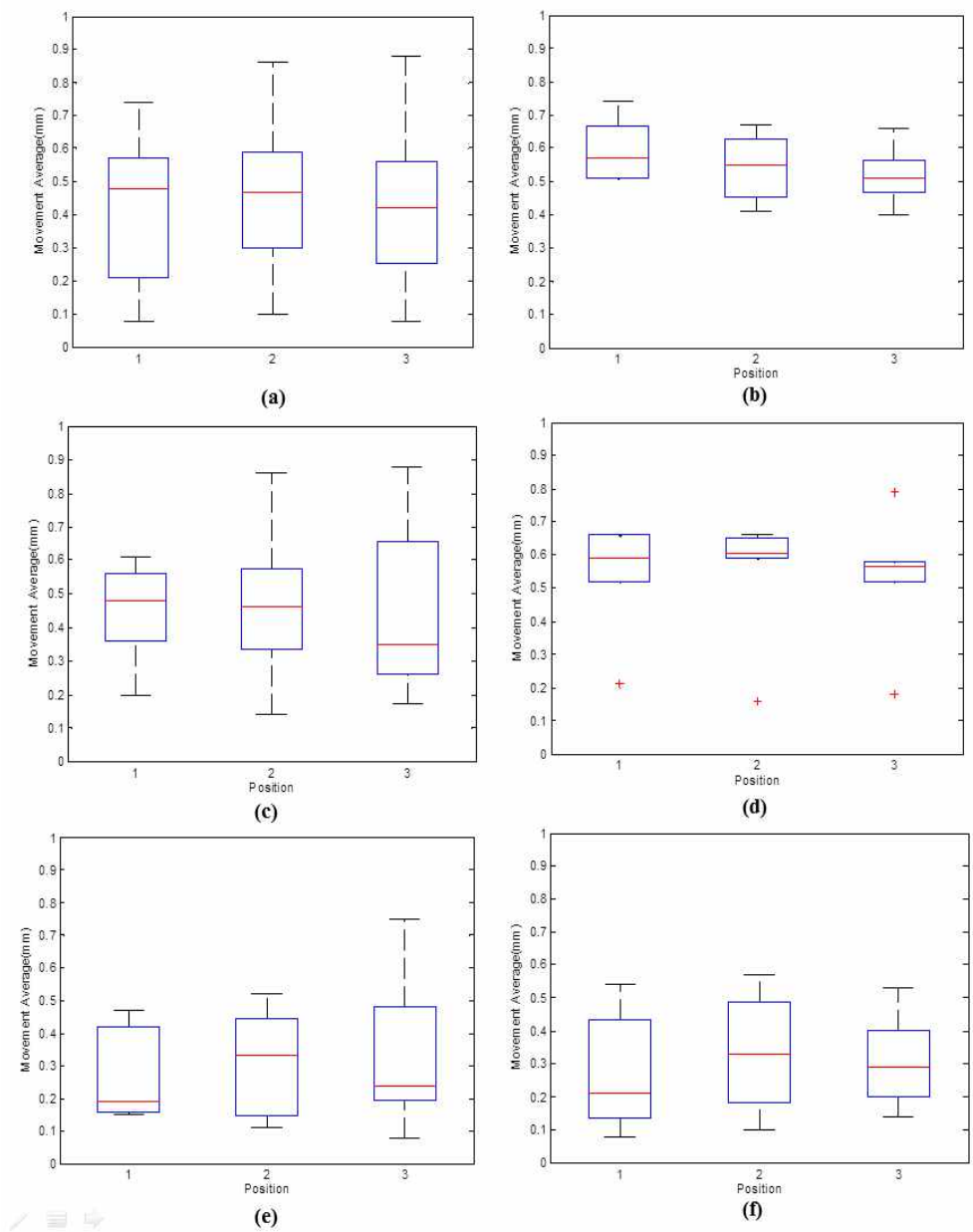

Figure 6.8 The boxplot of each thoracic aorta movement distance at their age group (a) subject total (b) 30s (c) 40s (d) 50s (e) 60s (f) 70s and over

6.1.6. Aortic Displacement and Position

In this section, aortic displacement were investigated with selected subjects. For inclusion into this study, the images had to possible to evaluate the ascending and descending aorta. The nine case was suitable for assessment from the study population.

Table 6.4 represents the aortic displacement in each aorta position. The displacement data are presented as mean ± S.D.

Figure 6.9 shows the aortic displacement comparison of the selected subjects for this investigation. Displacement was greater at ascending aorta compared to descending aorta. No differences were found among the descending aorta. Figure 6.10 shows the aorta displacement magnitude and direction. Figure 6.10 (a) and 6.10 (b) represents 44-year-old female and 78-year-old male aorta, respectively. The younger person had different aorta motion property which is an acute angle of displacement.

Table 6.4 Aortic displacement in each aorta position

No.	Subject No.	Age	Position	Displacement summation (mm)	Displacement Mean ± SD (mm)
1	1	49	Asc.	14.37	0.72 ± 0.59
			Desc. 1st	2.49	0.12 ± 0.04
			Desc. 2nd	6.54	0.33 ± 0.15
			Desc. 3rd	3.61	0.18 ± 0.10
2	2	66	Asc.	8.76	0.44 ± 0.25
			Desc. 1st	1.69	0.08 ± 0.06
			Desc. 2nd	3.5	0.17 ± 0.12
			Desc. 3rd	10.16	0.51 ± 0.24
3	4	49	Asc.	18.76	0.94 ± 0.58
			Desc. 1st	4.72	0.24 ± 0.12
			Desc. 2nd	3.14	0.16 ± 0.12
			Desc. 3rd	8.09	0.40 ± 0.33
4	5	47	Asc.	15.19	0.76 ± 0.46
			Desc. 1st	4.83	0.24 ± 0.15
			Desc. 2nd	4.7	0.24 ± 0.13
			Desc. 3rd	5.58	0.28 ± 0.18
5	9	44	Asc.	7.74	0.39 ± 0.56
			Desc. 1st	1.72	0.09 ± 0.09
			Desc. 2nd	2.41	0.12 ± 0.08
			Desc. 3rd	2.85	0.14 ± 0.11
6	10	78	Asc.	11.77	0.59 ± 0.31
			Desc. 1st	3.11	0.16 ± 0.07
			Desc. 2nd	2.37	0.12 ± 0.05
			Desc. 3rd	3.65	0.18 ± 0.10
7	14	55	Asc.	13.93	0.70 ± 0.62
			Desc. 1st	5.17	0.27 ± 0.18
			Desc. 2nd	4.27	0.21 ± 0.12
			Desc. 3rd	5.27	0.26 ± 0.12

8	16	50	Asc.	22.72	1.14 ± 0.71
			Desc. 1st	5.66	0.28 ± 0.18
			Desc. 2nd	5.18	0.26 ± 0.10
			Desc. 3rd	9.86	0.49 ± 0.22
9	19	77	Asc.	9.25	0.46 ± 0.29
			Desc. 1st	4.07	0.20 ± 0.10
			Desc. 2nd	4.45	0.22 ± 0.14
			Desc. 3rd	6	0.30 ± 0.25

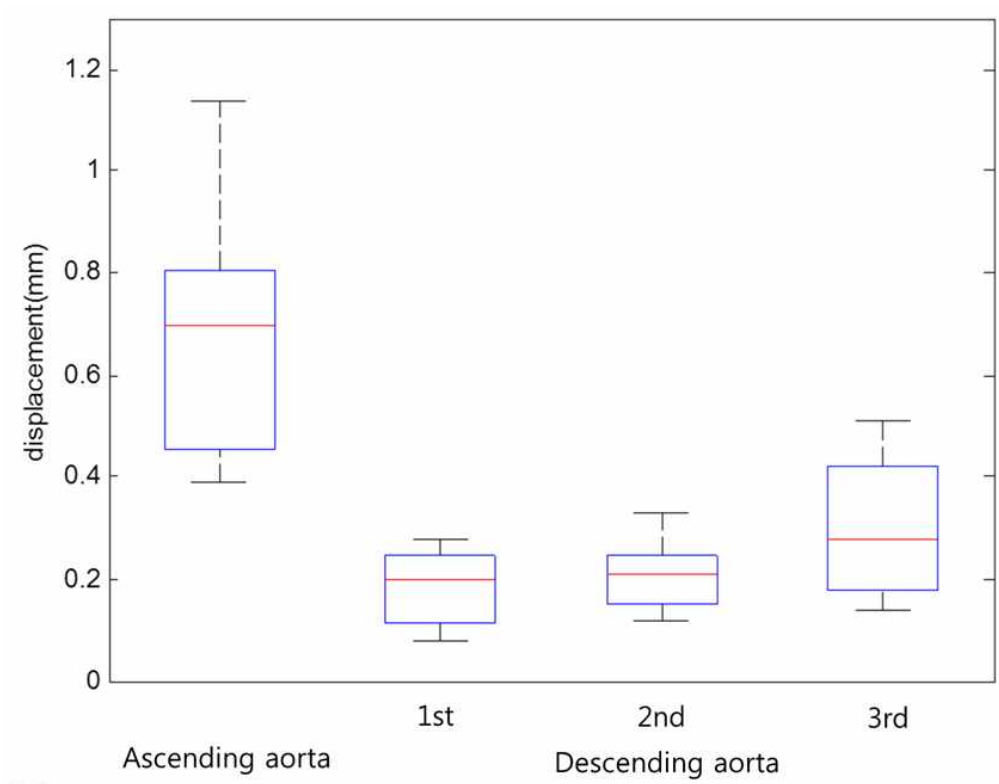

Figure 6.9 Aortic displacement comparison of the subjects

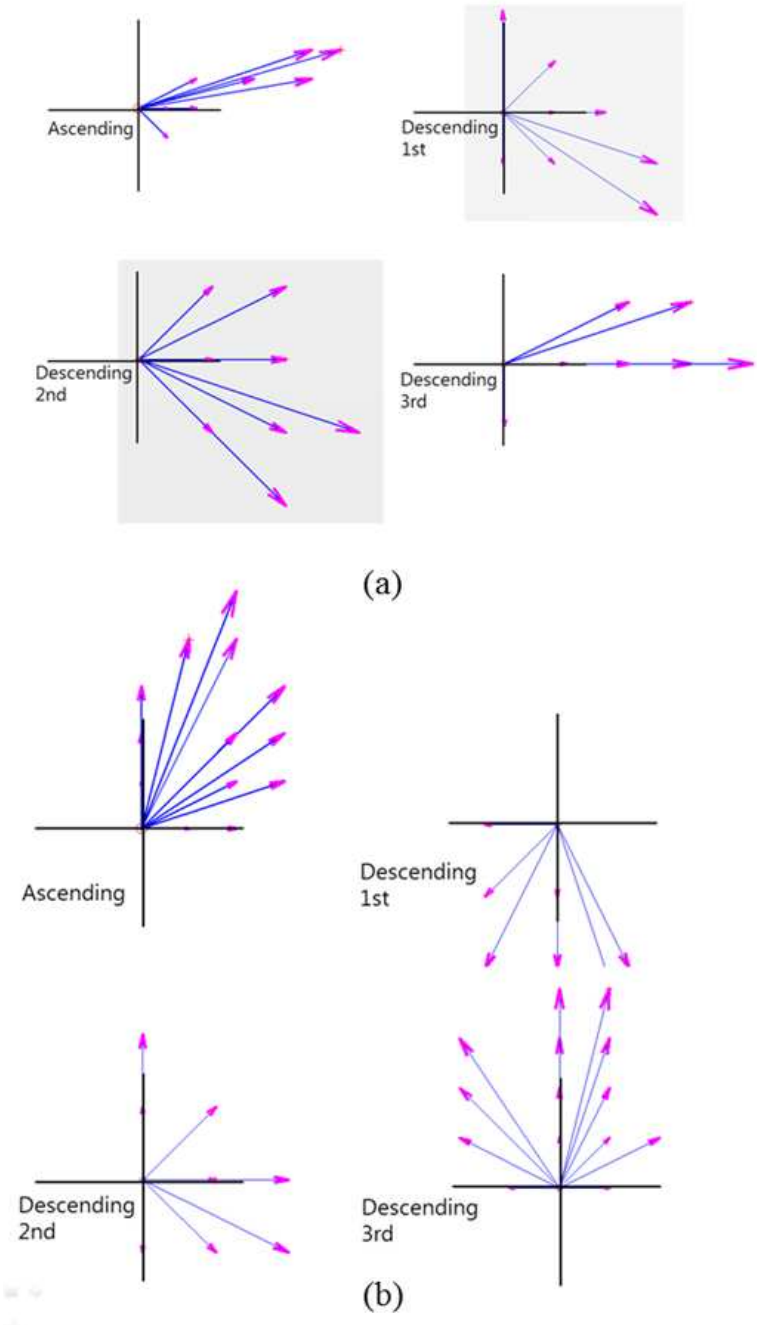

Figure 6.10 Aorta displacement magnitude and direction
(a) 44-year-old female aorta displacement
(b) 78-year-old male aorta displacement

6.1.7. Discussion

In this chapter, various assessment topics were employed to identify the feasibility of dynamic aorta motion analysis using MDCT images. This study reports on wall movement, magnitude and direction of the displacement of the aorta in patients. The results showed the new visualization method for dynamic aorta motion and property.

There was a significant decrease of the aortic wall motion at all thoracic levels throughout the ages. Although specific assessment of vascular aging was not available for the diseased subjects, a potential distinction on the aorta aging at the different ages was possible.

In contrast to the ascending aorta, the descending segments presented a significantly lesser magnitude of displacement and appear rather fixed at their thoracic position.

Although the proposed clinical validation showed the aorta motion property, it is required to evaluate enough large database of normal subjects.

6.2. Aorta Motion Assessment using Cine-MR Images

6.2.1. Subject and Image Data

The aorta images of 17 subjects (17 women; mean age, 21.6 ± 6.6 years; range, 11-38 years) who underwent aorta scanning during period February 2011 to July 2011 at Severance hospital were recruited in this study. The MR data of all subjects were collected during 5 month.

All images of 14 subjects from MR were reviewed and sampled by radiologist. Table 6.2 shows the clinical characteristics of the subjects and acquired image frames.

Table 6.5 Subjects and MR image data of study population

Subject No.	Age	Sex	Position	Frame	Pixel Spacing (mm)
1	20	F	1st	60	1.25
			2nd	50	
			3rd	50	
2	26	F	1st	60	1.25
			2nd	60	
			3rd	60	
3	34	F	1st	60	1.25
			2nd	50	
			3rd	50	
4	22	F	1st	60	1.25
			2nd	60	
			3rd	60	
5	21	F	1st	60	1.25
			2nd	60	
			3rd	60	

6	21	F	1st	60	1.25
			2nd	60	
			3rd	60	
7	11	F	1st	60	1.02
			2nd	60	
			3rd	60	
8	17	F	1st	60	1.25
			2nd	60	
			3rd	60	
9	38	F	1st	60	1.48
			2nd	60	
			3rd	60	
10	28	F	1st	60	1.25
			2nd	60	
			3rd	60	
11	31	F	1st	60	1.25
			2nd	60	
			3rd	60	
12	23	F	1st	60	1.25
			2nd	60	
			3rd	60	
13	20	F	1st	60	1.25
			2nd	60	
			3rd	60	
14	25	F	1st	60	1.25
			2nd	60	
			3rd	60	
15	17	F	1st	60	1.25
			2nd	60	
			3rd	60	
16	12	F	1st	60	1.25
			2nd	60	
			3rd	50	
17	14	F	1st	60	1.25
			2nd	60	
			3rd	60	

6.2.2. Aortic Wall Movement in Cine-MR Images

In this section, the wall movement distance of descending aorta using Cine-MR images were calculated and depicted. To demonstrated this outcome, descending aorta boundary segmentation and wall motion tracking were performed. Figure 6.11 shows the results of wall motion tracking by proposed algorithms. The magnitude of wall movement velocity throughout the cardiac cycle was obtained. The point velocity was classified into three groups; red, green, blue. The colors were assigned by wall movement distance in order. The red clustered point means the fastest variation among the three groups. The green and blue represented the second and third group. Figure 6.12 shows example of wall movement profiles. Figure 6.12 (a) represents the every 48 wall points variations and figure 6.12 (b) shows the clustered points graph by vector velocity. The dashed red line with cross represented the fastest wall motion cluster. The dashed magenta line with circle and dashed blue line with cross was the second and the third cluster, respectively in figure 6.12 (b). The y-axis value of clustered points variation represents the mean variation in each frame. In figure 6.12 (b), the orange rectangular means the frame of aorta expansion. It corresponds with figure 6.12 (c).

The wall movement of descending aorta for total subjects were presented as mean ± standard deviation (S.D.) as shown in Table 6.5.

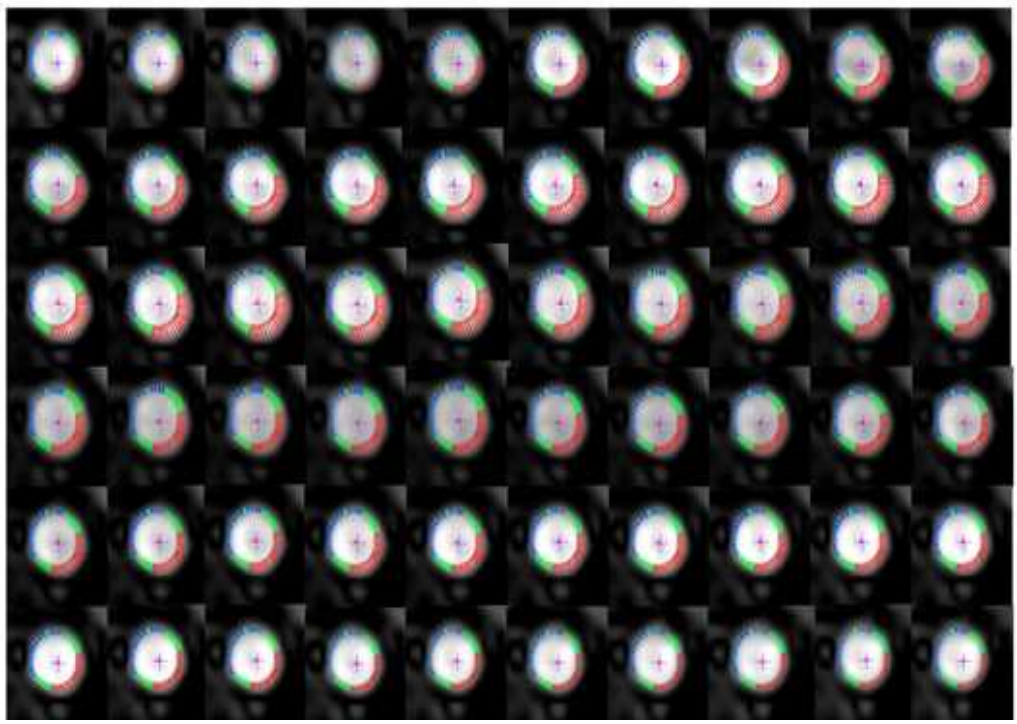

Figure 6.11 Example of phase MR images after mapping of vector velocity

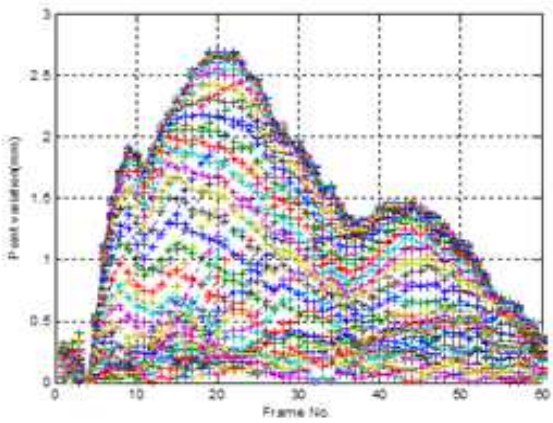

(a)

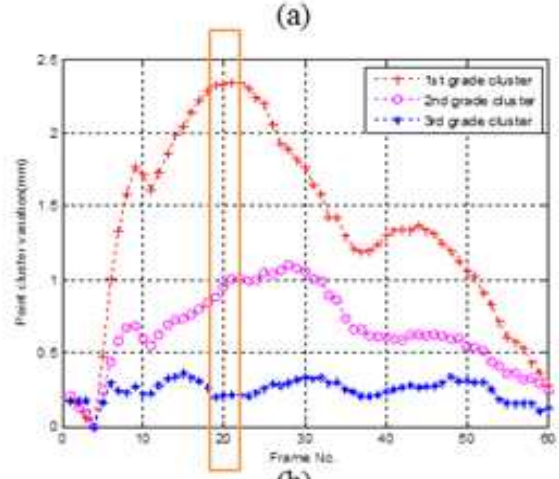

(b)

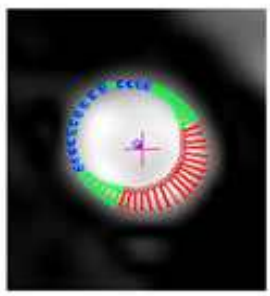

(c)

Figure 6.12 Example of aorta wall movement profiles at 2nd position of descending aorta (a) aorta wall variation graph (b) movement of clustered by velocity (c) vector velocity mapping when descending aorta expansion

Table 6.6 Subjects and wall movement in Turner syndrome

Subject No.	Age	Position	Point Movement Average (mm)			
			All	First	Second	Third
			Mean ± SD	Mean ± SD	Mean ± SD	Mean ± SD
1	20	1st	1.04 ± 0.36	1.44 ± 0.87	0.94 ± 0.41	0.62 ± 0.28
		2nd	0.58 ± 0.36	0.99 ± 0.67	0.41 ± 0.26	0.23 ± 0.09
		3rd	0.50 ± 0.37	0.92 ± 0.71	0.31 ± 0.23	0.14 ± 0.08
2	26	1st	1.32 ± 0.68	2.05 ± 1.01	1.19 ± 0.50	0.49 ± 0.20
		2nd	0.57 ± 0.38	1.00 ± 0.60	0.39 ± 0.22	0.17 ± 0.07
		3rd	0.56 ± 0.36	0.95 ± 0.63	0.46 ± 0.29	0.15 ± 0.07
3	34	1st	0.68 ± 0.36	1.06 ± 0.60	0.60 ± 0.32	0.25 ± 0.15
		2nd	0.71 ± 0.37	1.12 ± 0.75	0.58 ± 0.34	0.31 ± 0.12
		3rd	0.65 ± 0.24	0.92 ± 0.77	0.58 ± 0.46	0.37 ± 0.27
4	22	1st	0.75 ± 0.37	1.15 ± 0.65	0.64 ± 0.35	0.35 ± 0.13
		2nd	0.48 ± 0.28	0.76 ± 0.49	0.43 ± 0.18	0.14 ± 0.05
		3rd	0.46 ± 0.30	0.79 ± 0.54	0.34 ± 0.24	0.15 ± 0.08
5	21	1st	1.10 ± 0.22	1.31 ± 0.61	1.03 ± 0.42	0.89 ± 0.40
		2nd	0.68 ± 0.13	0.80 ± 0.62	0.65 ± 0.24	0.54 ± 0.20
		3rd	0.53 ± 0.34	0.90 ± 0.65	0.45 ± 0.30	0.13 ± 0.07
6	21	1st	0.84 ± 0.36	0.20 ± 0.83	0.79 ± 0.24	0.39 ± 0.23
		2nd	0.59 ± 0.36	0.99 ± 0.77	0.42 ± 0.20	0.21 ± 0.12
		3rd	0.80 ± 0.41	1.22 ± 0.74	0.74 ± 0.43	0.29 ± 0.15
7	11	1st	0.54 ± 0.18	0.72 ± 0.52	0.49 ± 0.26	0.34 ± 0.15
		2nd	0.62 ± 0.30	0.93 ± 0.45	0.55 ± 0.27	0.26 ± 0.11
		3rd	0.54 ± 0.35	0.93 ± 0.51	0.41 ± 0.23	0.16 ± 0.07
8	17	1st	0.86 ± 0.60	1.53 ± 0.79	0.58 ± 0.33	0.26 ± 0.13
		2nd	0.39 ± 0.22	0.63 ± 0.41	0.33 ± 0.18	0.12 ± 0.05
		3rd	0.57 ± 0.28	0.87 ± 0.61	0.53 ± 0.33	0.23 ± 0.10
9	38	1st	0.66 ± 0.32	1.01 ± 0.50	0.57 ± 0.28	0.29 ± 0.09
		2nd	0.36 ± 0.23	0.62 ± 0.44	0.23 ± 0.10	0.16 ± 0.06
		3rd	0.52 ± 0.30	0.86 ± 0.58	0.37 ± 0.27	0.21 ± 0.13
10	28	1st	0.47 ± 0.15	0.61 ± 0.30	0.49 ± 0.17	0.26 ± 0.11
		2nd	0.48 ± 0.26	0.76 ± 0.48	0.41 ± 0.21	0.19 ± 0.07
		3rd	0.41 ± 0.23	0.66 ± 0.48	0.35 ± 0.22	0.14 ± 0.07

11	31	1st	0.24 ± 0.31	0.87 ± 0.44	0.44 ± 0.21	0.19 ± 0.11
		2nd	0.49 ± 0.34	0.87 ± 0.59	0.35 ± 0.18	0.13 ± 0.04
		3rd	0.51 ± 0.31	0.83 ± 0.70	0.43 ± 0.25	0.15 ± 0.07
12	23	1st	0.88 ± 0.59	1.47 ± 0.61	0.62 ± 0.25	0.37 ± 0.15
		2nd	0.68 ± 0.38	1.09 ± 0.65	0.58 ± 0.28	0.26 ± 0.14
		3rd	0.59 ± 0.46	1.10 ± 0.69	0.38 ± 0.22	0.13 ± 0.05
13	20	1st	0.76 ± 0.33	1.12 ± 0.87	0.65 ± 0.42	0.38 ± 0.19
		2nd	0.80 ± 0.56	1.42 ± 0.86	0.50 ± 0.36	0.27 ± 0.18
		3rd	0.68 ± 0.55	1.29 ± 0.82	0.37 ± 0.19	0.17 ± 0.10
14	25	1st	0.77 ± 0.37	1.16 ± 0.55	0.65 ± 0.27	0.35 ± 0.16
		2nd	0.49 ± 0.36	0.89 ± 0.51	0.33 ± 0.17	0.11 ± 0.06
		3rd	0.40 ± 0.27	0.69 ± 0.47	0.31 ± 0.20	0.09 ± 0.04
15	17	1st	0.97 ± 0.58	1.59 ± 1.03	0.80 ± 0.35	0.31 ± 0.15
		2nd	0.89 ± 0.68	1.65 ± 0.83	0.57 ± 0.28	0.21 ± 0.08
		3rd	0.07 ± 0.50	1.24 ± 0.86	0.57 ± 0.38	0.12 ± 0.07
16	12	1st	0.82 ± 0.50	1.37 ± 0.65	0.65 ± 0.27	0.25 ± 0.07
		2nd	0.81 ± 0.51	1.37 ± 0.76	0.62 ± 0.29	0.26 ± 0.09
		3rd	0.64 ± 0.38	1.04 ± 0.64	0.55 ± 0.29	0.17 ± 0.08
17	14	1st	0.65 ± 0.37	1.40 ± 0.68	0.52 ± 0.31	0.25 ± 0.10
		2nd	0.41 ± 0.27	0.71 ± 0.58	0.31 ± 0.14	0.11 ± 0.04
		3rd	0.52 ± 0.34	0.89 ± 0.64	0.40 ± 0.21	0.15 ± 0.08

6.2.3. Aortic Wall Movement and Age in Turner Syndrome

The scatter plots and Pearson's correlation coefficients of between three different position of descending aorta and ages in Turner syndrome subjects are investigated. The averaged wall movement at 1st position of descending aorta along the entire study population groups in figure 6.13 and the correlation coefficient was -0.22 ($p = 0.40$). Figure 6.14 shows the averaged aortic wall movement at the 2nd position of descending aorta along the entire study population groups and the correlation coefficient was -0.33 ($p = 0.19$). Figure 6.15 represents averaged aortic wall movement at the 3rd position of descending aorta along the entire study population groups and the correlation coefficient was 0.04 ($p = 0.90$).

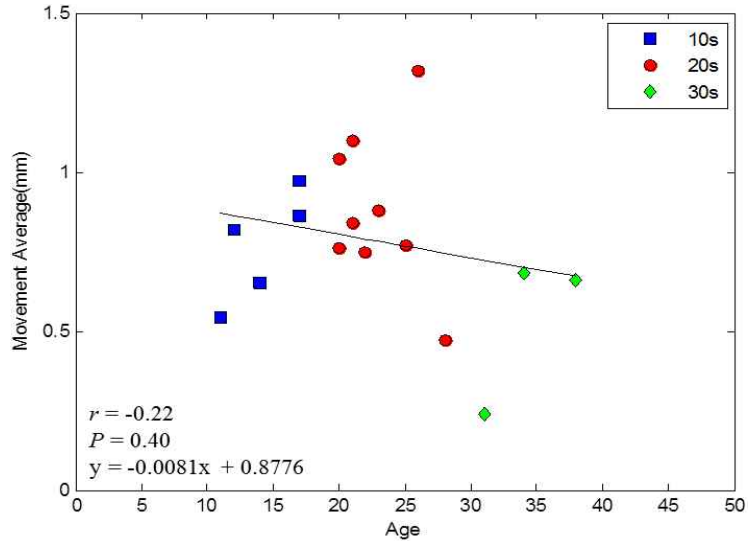

Figure 6.13 Correlation between age and averaged wall movement of thoracic aorta at 1st position in Turner syndrome

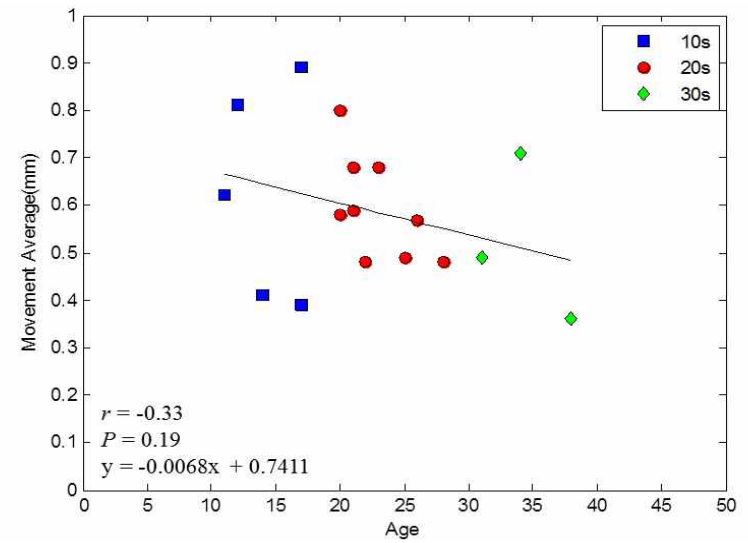

Figure 6.14 Correlation between age and averaged wall movement of thoracic aorta at 2nd position in Turner syndrome

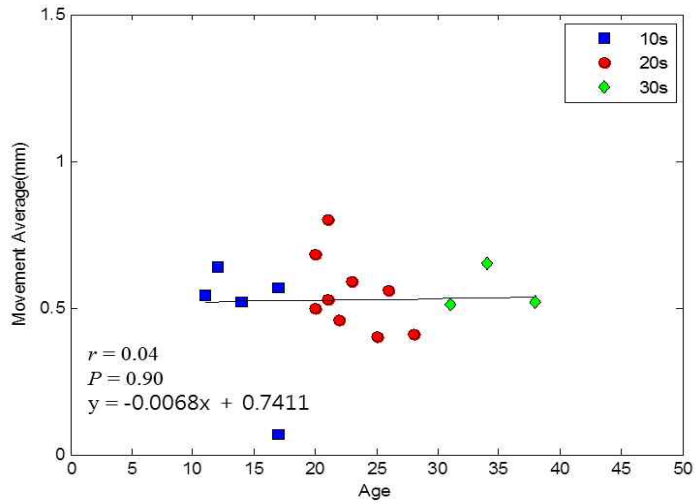

Figure 6.15 Correlation of age and averaged wall movement of thoracic aorta at 3rd position in Turner syndrome

6.2.4. Aortic Wall Movement and Position in Turner Syndrome

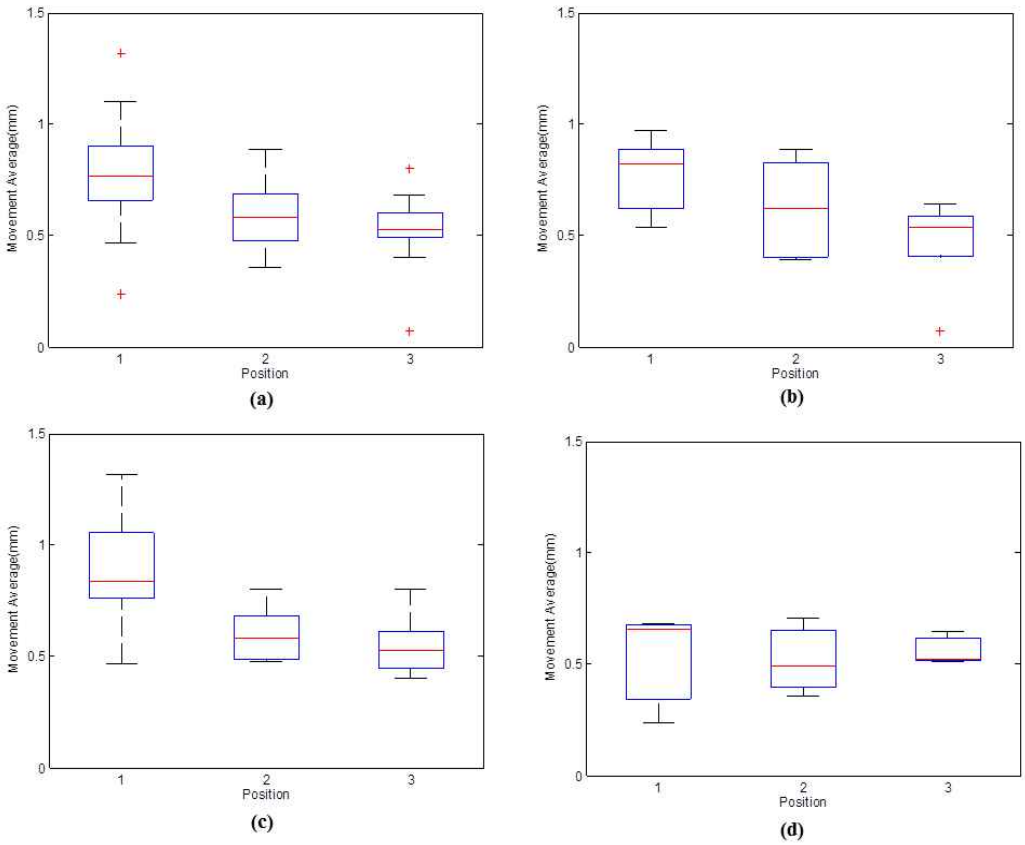

Figure 6.16 The boxplot of descending aorta movement in each position at their age group (a) subject total (b) 10s (c) 20s (d) 30s

Figure 6.16 is the boxplot of descending aorta movement according to age group. There was significant decrease of the movement at different thoracic levels in total. This tendency also exists in each age group. The more subjects will be investigated for accurate statistical analysis.

6.2.5. Discussion

In this chapter, various assessment topics were employed to identify the feasibility of dynamic aorta motion analysis using Cine-MR images. This study reports on wall movement, magnitude and direction of the displacement of the aorta in Turner Syndrome. The results showed the new visualization method for dynamic aorta motion and property.

Although specific assessment of aorta elasticity was not available for the diseased subjects that were studied, a potential distinction on the aortic elasticity at the different thoracic levels was possible.

In contrast to the 1st descending aorta, the 2nd and 3rd segments presented a significantly lesser magnitude of displacement and appear rather fixed at their position.

Although the proposed clinical validation showed the aorta motion property, it is required to evaluate enough large database of normal subjects.

Chapter 7

7. Conclusions

A new approach for visualization and blood vessel motion assessment cross-sectional images of aorta were presented throughout this study. In this chapter, the summary and conclusion of this study will be provided.

7.1. Summary

The proposed image processing strategies for blood vessel radial motion were adapted to sequential images from different modalities. The principal findings of this study are follows.

(1) Blood vessel wall motion could be visualization under specific image acquisition protocols.

(2) Vector velocity mapping provide the quantitative evaluation of blood vessel motion include regional and global aspects.

(3) Wall motion distance profiles could be a clue for distinction between normal blood vessel and abnormal.

(4) Sequential contrast enhanced blood vessel images from even different modality adapted to evaluate the mechanical function.

These findings suggest that aorta assessment using proposed algorithms and assessment strategy may represent a new method for non-invasively quantifying vascular mechanical functions.

7.2. Clinical Impacts of the Study

The proposed algorithm is a promising tool as quantitative assessment method to evaluate the function of blood vessel motion. It is not only providing the parametric values for assessment vascular but also suggests qualitative screening intuition.

In aorta assessment using MDCT images, although clinical validation design included a limited number of subjects, each subject served as his or her own comparator. Consequently, we were able to detect significant differences between groups. The subject population included mainly patients with valvular disease. Therefore the results do not necessarily apply to patients without cardiac disease. In addition the patient population was relatively homogenous in terms of baseline characteristics (age and sex).

In aorta assessment using MR images, although specific diagnoses were not available for the subjects that were studied, a clear description on the aortic movement profiles throughout subject population.

There was a significant decrease of the aortic wall motion at all thoracic

levels throughout the ages. Although specific assessment of vascular aging was not available for the diseased subjects, a potential distinction on the aorta aging at the different ages was possible.

In contrast to the ascending aorta, the descending segments presented a significantly lesser magnitude of displacement and appear rather fixed at their thoracic position.

The results of this dissertation provide the fundamental characteristics of blood vessel motion and could be used not only clinical researches also clinical applications, such as vascular aging, assessment of vascular disease, and early detection of vascular abnormality.

7.3. Future Works

This dissertation demonstrates the method to assess the aorta motion. The image processing steps were developed and applied to sequential MDCT and MR images. Although the proposed algorithm showed suitable performance to evaluate the wall motion, there still remain challenges to improve.

The image processing method has inherent difference of inter- and intra-observer variability. The semi–automatic selection of wall boundary has to be improving to reduce the variability. The wall boundary is sampled and interpolated by user however, automatic image processing should be studied. In addition, noise robust algorithms has to be considered.

The reference data of aorta wall motion was assessed using a small number of diseased subjects. It is required to evaluate with large data in long term and normal subjects.

References

[1] A. F. Frangi, *et al.*. "Vascular Imaging". *Medical Imaging, IEEE Transactions on*, 24(4): pp. 433-435, 2005.

[2] P. Reimer and P. Landwehr, "Non-invasive vascular imaging of peripheral vessels," *European Radiology*, vol. 8, pp. 858-872, 1998.

[3] N. E. Green, *et al.*, "Three-dimensional vascular angiography," *Current Problems in Cardiology*, vol. 29, pp. 104-142, 2004.

[4] V. L. Rowe and S. W. Tucker Jr, "Advances in vascular imaging," *The Surgical clinics of North America*, vol. 84, p. 1189, 2004.

[5] P. N. T. Wells, "Current status and future technical advances of ultrasonic imaging," *Engineering in Medicine and Biology Magazine, IEEE*, vol. 19, pp. 14-20, 2000.

[6] M. H. R. Cardinal, *et al.*, "Fast-marching segmentation of three-dimensional intravascular ultrasound images: A pre-and post-intervention study," *Medical physics*, vol. 37, p. 3633, 2010.

[7] C. Catalano, *et al.*, "MDCT of the abdominal aorta: basics, technical improvements, and clinical applications," *European Radiology*, vol. 13, pp. 53-58, 2003.

[8] H. Cline, *et al.*, "Coronary artery angiography using multislice computed tomography images," *Circulation*, vol. 102, pp. 1589-1590, 2000.

[9] J. K. Willmann, *et al.*, "Aortoiliac and Renal Arteries: Prospective

Intraindividual Comparison of Contrast-enhanced Three-dimensional MR Angiography and Multi‐Detector Row CT Angiography," *Radiology*, vol. 226, pp. 798-811, 2003.

[10] R. Gebker, *et al.*, “Diagnostic performance of myocardial perfusion MR at 3 T in patients with coronary artery disease,” *Radiology,* 247:57‐63, 2008.

[11] JS. Lindholt, *et al.*, “Screening for abdominal aortic aneurysms: single center randomized controlled trial,” *BMJ*, 330:750, 2005.

[12] J. Takasu, *et al.*, "Aortic atherosclerosis detected with electron-beam CT as a predictor of obstructive coronary artery disease," *Academic radiology*, vol. 10, pp. 631-637, 2003.

[13] N. D. Wong, *et al.*, "Thoracic aortic calcium versus coronary artery calcium for the prediction of coronary heart disease and cardiovascular disease events," *JACC: Cardiovascular Imaging*, vol. 2, pp. 319-326, 2009.

[14] F. Y. Lin, *et al.*, "Assessment of the thoracic aorta by multidetector computed tomography: age-and sex-specific reference values in adults without evident cardiovascular disease," *Journal of Cardiovascular Computed Tomography*, vol. 2, pp. 298-308, 2008.

[15] N. D. Wong, *et al.*, "Thoracic aortic calcium versus coronary artery calcium for the prediction of coronary heart disease and cardiovascular disease events," *JACC: Cardiovascular Imaging*, vol. 2, pp. 319-326, 2009.

[16] L. Yang, *et al.*, "64-MDCT coronary angiography of patients with atrial fibrillation: influence of heart rate on image quality and efficacy in evaluation of coronary artery disease," *American Journal of Roentgenology*, vol. 193, pp. 795-801, 2009.

[17] R. K. Johnson, *et al.*, "Quantitative assessment of the entire thoracic aorta from magnetic resonance images," *Cardiology in the Young*, vol. 21, pp. 170-177, 2011.

[18] A. Herment, *et al.*, "Comparison of aortic lumen area and distensibility using cine and phase contrast acquisitions," *Proc. of Computing in Cardiology*, pp. 173-176, 2010.

[19] F. Lauze and M. de Bruijne, "Toward automated detection and segmentation of aortic calcifications from radiographs," *Proc. of SPIE* Vol. 6512, 2007.

[20] M. Jeltsch, *et al.*, "Aortic wall thickness assessed by multidetector computed tomography as a predictor of coronary atherosclerosis," T*he International Journal of Cardiovascular Imaging (formerly Cardiac Imaging)*, vol. 25, pp. 209-217, 2009.

[21] J. K. Song, *et al.*, "Different clinical features of aortic intramural hematoma versus dissection involving the ascending aorta," *Journal of the American College of Cardiology*, vol. 37, pp. 1604-1610, 2001.

[22] J. A. Elefteriades, "Natural history of thoracic aortic aneurysms: indications for surgery, and surgical versus nonsurgical risks," *The Annals of thoracic surgery*, vol. 74, pp. S1877-S1880, 2002.

[23] G. J. Nollen, *et al.*, "Aortic stiffness and diameter predict progressive aortic dilatation in patients with Marfan syndrome," *European heart journal*, vol. 25, p. 1146, 2004.

[24] D. T. Boll, *et al.*, "Synergy of MDCT and cine MRI for the evaluation of cardiac motility," *American Journal of Roentgenology*, vol. 186, pp. S379-S386, 2006.

[25] E. Konen, *et al.*, "The role of ECG-gated MDCT in the evaluation of aortic and mitral mechanical valves: initial experience," *American Journal of Roentgenology*, vol. 191, pp. 26-31, 2008.

[26] L. Yang, *et al.*, "64-MDCT coronary angiography of patients with atrial fibrillation: influence of heart rate on image quality and efficacy in evaluation of coronary artery disease," *American Journal of Roentgenology*, vol. 193, pp. 795-801, 2009.

[27] C. Catalano, *et al.*, "MDCT of the abdominal aorta: basics, technical improvements, and clinical applications," *European Radiology*, vol. 13, pp. 53-58, 2003.

[28] E. Robertson, "Cardiac Imaging－Technical Advances in MDCT Compared with Conventional X-ray Angiography," pp. 1-5, 2005.

[29] F. Rengier, *et al.*, "Centerline analysis of aortic CT angiographic examinations: benefits and limitations," *American Journal of Roentgenology*, vol. 192, pp. W255-W263, 2009.

[30] T. Kido, *et al.*, "Cardiac imaging using 256-detector row four-dimensional CT: preliminary clinical report," *Radiation medicine*,

vol. 25, pp. 38-44, 2007.

[31] I. Macía, *et al.*, "Segmentation of abdominal aortic aneurysms in CT images using a radial model approach," *Proc. of IDEAL'09 Proceedings of the 10th international conference on Intelligent data engineering and automated learning*, pp. 664-671, 2009.

[32] L. R. Varshney, "Abdominal Organ Segmentation in CT Scan Images: A Survey," 2002.

[33] S. Wang, "Clinical Applications of Cardiac Multi-detector Computed Tomography," pp. 1-169, 2011.

[34] M. E. Clouse, *et al.*, "Measuring noncalcified coronary atherosclerotic plaque using voxel analysis with MDCT angiography: a pilot clinical study," *American Journal of Roentgenology*, vol. 190, pp. 1553-1560, 2008.

[35] L. Gerace, "Detection of Abdominal Aortic Calcification with IVA," pp. 1-4, 2006.

[36] R. C. Gilkeson, *et al.*, "MDCT evaluation of aortic valvular disease," *American Journal of Roentgenology*, vol. 186, pp. 350-360, 2006.

[37] S. Golemati, *et al.*, "Carotid artery wall motion estimated from B-mode ultrasound using region tracking and block matching," *Ultrasound in medicine & biology*, vol. 29, pp. 387-399, 2003.

[38] B. Ibáñez, *et al.*, "Novel Imaging Techniques for Quantifying Overall Atherosclerotic Burden:: Non-Coronary Arterial Disease (II)," *Revista Española de Cardiología*, vol. 60, pp. 299-309, 2007.

[39] P. Raggi, *et al.*, "Atherosclerotic plaque imaging: contemporary role in preventive cardiology," *Archives of internal medicine*, vol. 165, p. 2345, 2005.

[40] K.-S. Cheng, *et al.*, "Arterial elastic properties and cardiovascular risk/event.". *European journal of vascular and endovascular surgery : the official journal of the European Society for Vascular Surgery*, 24(5): pp. 383-397, 2002.

[41] K. S. Cheng, *et al.*, "Arterial elastic properties and cardiovascular risk/event," *European journal of vascular and endovascular surgery*, vol. 24, pp. 383-397, 2002.

[42] M. J. Lipinski *et al.,* "Atherosclerotic Plaque Imaging," *MRI and CT of the cardiov ascular system*, p. 361, 2006.

[43] M. Ganten, *et al.*, "Age related changes of human aortic distensibility: evaluation with ECG-gated CT," *European Radiology*, vol. 17, pp. 701-708, 2007.

[44] M. K. Ganten, *et al.*, "Quantification of aortic distensibility in abdominal aortic aneurysm using ECG-gated multi-detector computed tomography," *European Radiology*, vol. 18, pp. 966-973, 2008.

[45] U. Kurkure, *et al.*, "Automated segmentation of thoracic aorta in non-contrast CT images," *Proc. of Biomedical Imaging: From Nano to Macro, 2008. ISBI 2008. 5th IEEE International Symposium on*, pp. 29-32, 2008.

[46] J. K. Johnstone and K. R. Sloan, "Visualization of LV wall motion

and thickness from MRI data," *Proc. of Computers in Cardiology*, pp. 249-252, 1995.

[47] M. J. McKeown, *et al.*, "Spatially independent activity patterns in functional MRI data during the Stroop color-naming task," *Proceedings of the National Academy of Sciences*, vol. 95, p. 803, 1998.

[48] J. Rose, *et al.*, "Automatic detection of vessel wall contours from cine-MRI for aortic compliance determination," *Proc. of Computers in Cardiology*, pp. 411-414, 2005.

[49] I. M. Adame, *et al.*, "Automatic vessel wall contour detection and quantification of wall thickness in vivo MR images of the human aorta," *Journal of Magnetic Resonance Imaging*, vol. 24, pp. 595-602, 2006.

[50] R. P. Choudhury, *et al.*, "MRI and characterization of atherosclerotic plaque," *Arteriosclerosis, thrombosis, and vascular biology*, vol. 22, pp. 1065-1074, 2002.

[51] R. Corti, *et al.*, "In vivo noninvasive detection and age definition of arterial thrombus by MRI," *Journal of the American College of Cardiology*, vol. 39, p. 1366, 2002.

[52] T. Chen, *et al.*, "Semiautomated segmentation of myocardial contours for fast strain analysis in cine displacement-encoded MRI," *Medical Imaging, IEEE Transactions on*, vol. 27, pp. 1084-1094, 2008.

[53] L. Florack and H. van Assen, "Direct computation of myocardial deformation and strain from tagged cine MRI," 2008.

[54] L. Imanirad, "Segmentation and Tracking of the Left Ventricle in Cardiac MRI," *University of Toronto*, 2006.

[55] M. Katoh, *et al.*, "MRI of coronary vessel walls using radial k-space sampling and steady-state free precession imaging," *American Journal of Roentgenology*, vol. 186, pp. S401-S406, 2006.

[56] J. Rose, *et al.*, "Automatic detection of vessel wall contours from cine-MRI for aortic compliance determination," *Proc. of Computers in Cardiology*, pp. 411-414, 2005.

[57] A. Herment, *et al.*, "Automated segmentation of the aorta from phase contrast MR images: validation against expert tracing in healthy volunteers and in patients with a dilated aorta," *Journal of Magnetic Resonance Imaging*, vol. 31, pp. 881-888, 2010.

[58] A. Wanhainen, *et al.*, "Thoracic and abdominal aortic dimension in 70-year-old men and women-A population-based whole-body magnetic resonance imaging (MRI) study," *Journal of Vascular Surgery*, vol. 47, pp. 504-512, 2008.

[59] G. MacLaren, *et al.*, "Comparative feasibility of myocardial velocity and strain measurements using 2 different methods with transesophageal echocardiography during cardiac surgery," *Journal of Cardiothoracic and Vascular Anesthesia*, vol. 25, pp. 216-220, 2011.

[60] K. Masuda, *et al.*, "Assessment of dyssynchronous wall motion during acute myocardial ischemia using Velocity Vector Imaging," *JACC: Cardiovascular Imaging*, vol. 1, pp. 210-220, 2008.

[61] F. A. Pac, *et al.*, "Wall motion velocities of ascending aorta measured by tissue Doppler imaging in obese children," *Pediatrics International*, vol. 52, pp. 778-784, 2010.

[62] R. Jurcut, *et al.*, "Detection of regional myocardial dysfunction in patients with acute myocardial infarction using velocity vector imaging," *Journal of the American Society of Echocardiography*, vol. 21, pp. 879-886, 2008.

[63] P. Tortoli, *et al.*, "A simplified approach for real-time detection of arterial wall velocity and distension," *Ultrasonics, Ferroelectrics and Frequency Control, IEEE Transactions on*, vol. 48, pp. 1005-1012, 2001.

[64] D. Hazarika, *et al.*, "Tracking of Heart Wall Motion using Unscented Kalman Filter," *Proc. of India Conference*, pp. 1-6, 2006.

[65] Johan, "Longitudinal Common Carotid Artery Wall Motion Mechanistic, prognostic and translational studies". pp. 1-60, 2011.

[66] M. S. Suffoletto, *et al.*, "Novel speckle-tracking radial strain from routine black-and-white echocardiographic images to quantify dyssynchrony and predict response to cardiac resynchronization therapy," *Circulation*, vol. 113, pp. 960-968, 2006.

[67] N. Li, *et al.*, "Assessment of thoracic aortic elasticity: a preliminary study using electrocardiographically gated dual-source CT," *European Radiology*, pp. 1-9, 2011.

[68] K. Koch, *et al.*, "Assessment of right ventricular function by

16-detector-row CT: comparison with magnetic resonance imaging," *European Radiology*, vol. 15, pp. 312-318, 2005.

[69] F. Y. Lin, *et al.*, "Assessment of the thoracic aorta by multidetector computed tomography: age-and sex-specific reference values in adults without evident cardiovascular disease," *Journal of Cardiovascular Computed Tomography*, vol. 2, pp. 298-308, 2008.

[70] F. Renard and Y. Yang, "Image analysis for detection of coronary artery soft plaques in MDCT images," *Proc. of Biomedical Imaging: From Nano to Macro, 2008. ISBI 2008. 5th IEEE International Symposium on*, pp. 25-28, 2008.

[71] C. Castro, *et al.*, "Coronary Artery Tracking in 3D Cardiac CT Images Using Local Morphological Reconstruction Operators," *The Insight Journal*, 2008.

[72] G. Heatlie and K. Pointon, "Cardiac magnetic resonance imaging," *Postgraduate medical journal*, vol. 80, pp. 19-22, 2004.

[73] N. Li, *et al.*, "Assessment of thoracic aortic elasticity: a preliminary study using electrocardiographically gated dual-source CT," *European Radiology*, pp. 1-9, 2011.

[74] T. Atherton and D. Kerbyson, "The coherent circle Hough transform," *Proc. of the British Machine Vision*, pp. 269-278, 1993.

[75] D. Ioannou, *et al.*, "Circle recognition through a 2D Hough transform and radius histogramming," *Image and Vision Computing*, vol. 17, pp. 15-26, 1999.

[76] L. Wang, *et al.*, "Fast iris localization based on improved Hough transform," *Rough Set and Knowledge Technology*, pp. 439-446, 2010.

[77] D. H. Ballard, "Generalizing the Hough transform to detect arbitrary shapes," *Pattern recognition*, vol. 13, pp. 111-122, 1981.

[78] A. Hager, *et al.*, "Diameters of the thoracic aorta throughout life as measured with helical computed tomography," *The Journal of thoracic and cardiovascular surgery*, vol. 123, p. 1060, 2002.

Abstract in Korean

MDCT와 Cine-MR 영상 분석을 통한 대동맥의 동적 특성 평가

연세대학교 대학원
의공학과
심 훈

본 논문은 대동맥의 동적 특성을 평가하기 위한 영상 처리 방법과 이를 이용한 임상적 응용에 대한 연구이다. 대동맥의 단면 영상을 이용하여 동적 특성 평가를 위한 분석 방법과 영상 획득 방법을 제안하였다.

대동맥의 동적 특성 평가를 위해 순차적인 단계의 영상 처리 방법을 적용 하였다. 첫째, 영상의 전처리로써 대동맥을 추출하기 위한 방법과 영상 확대 방법을 제안하였다. 둘째, 영상의 밝기 정보를 이용하여 대동맥의 경계벽을 추출 하였다. 셋째, 반 자동화 방법으로 여러 개의 영상 중 첫 번째 영상의 대동맥의 경계벽을 추출한 후 순차적으로 움직임을 추적 할 수 있도록 하였다. 또한, 대동맥의 움직임 정보를 시각화하고 정량화 하기 위하여 혈관벽에 벡터 속도를 나타내었다. 이 방법은 혈관벽의 움직임 속도와 혈관 자체의 움직임 정보를 정량적으로 표현한다.

본 논문에서 제안한 방법을 임상적인 적용을 위하여 MDCT와

Cine-MR 영상을 이용하였다.

MDCT 영상을 이용한 평가에서는 총 30명의 심판막 질환이 있는 피험자를 대상으로 대동맥 벽의 운동 특성, 석회화 된 대동맥 혈관벽의 움직임, 대동맥 벽의 움직임과 나이별 위치별 상관관계를 조사 하였다. 나이에 따른 대동맥 벽 움직임의 정도는 감소하는 것을 확인 하였다. 석회화가 있는 대동맥에서 벽의 움직임은 정상인 혈관 대비 움직임이 작은 것을 확인 하였다. 상행 대동맥과 하행 대동맥의 움직임 비교 평가에서는 상행 대동맥이 하행 대동맥 보다 혈관 자체의 움직임이 활발한 것을 확인 하였다.

MR 영상을 이용한 평가에서는 총 17명의 터너 증후군 피험자를 대상으로 대동맥 벽의 운동 특성과 하행 대동맥의 위치별 움직임의 차이를 확인 하였다. 하행 대동맥에서 가장 상단 부위에서 밑으로 내려갈수록 움직임이 작아지는 것을 확인 하였다.

본 논문의 결과는 영상 처리 방법을 이용하여 혈관 움직임의 동적 특성 평가 및 혈관 질환의 조기 발견을 위한 임상적 연구의 기초 자료로 활용될 수 있을 것으로 기대 된다. 추후 연구에서는 정상인을 대상으로 한 혈관 움직임 특성을 분석 한다면, 혈관의 노화와 질환별 혈관 움직임의 특성을 조기에 판단할 수 있을 것으로 판단한다.

핵심 단어 : 혈관 평가, 대동맥 기능 평가, 혈관벽 움직임, 다검출전산단층촬영, 자기공명영상